Application of a Site-Calibrated Parker-Klingeman Bedload Transport Model

Little Granite Creek, Wyoming

by

Mark R. Weinhold, P.E.

A thesis submitted in partial fulfillment of the requirements for the degree of

Masters of Science

Colorado State University

Fall 2001

Application of a Site-Calibrated Parker-Klingeman Bedload Transport Model

Little Granite Creek, Wyoming

by

Mark R. Weinhold, P.E.

A thesis submitted in partial fulfillment of the requirements for the degree of

Masters of Science

Colorado State University

Fall 2001

Approved by _____
Chairperson of Supervisory Committee

_____

_____

_____

Program Authorized
to Offer Degree _____

Date _____

ABSTRACT

Application of a Site-Calibrated Parker-Klingeman Bedload Transport Model

Little Granite Creek, Wyoming

by Mark R. Weinhold, P.E.

Chairperson of the Supervisory Committee: Professor Pierre Y. Julien
Department of Civil Engineering

The hiding effect between non-uniform sediment particles on a streambed is numerically quantified by an expression called the hiding factor, which relates critical Shields stresses to a ratio of particles sizes in the mixture of the bed. This hiding factor contains two parameters (P-K exponent and D_{50} reference shear) that will vary from stream to stream. This variability is what allows a bedload transport model, Parker-Klingeman in this case, to be site-calibrated using actual bedload measurements. The optimized value of the P-K exponent was found to be 0.973 at Little Granite Creek, compared to a value of unity for equal mobility. The value of the D_{50} reference shear, previously considered a constant, was shown to vary with discharge as a power function.

Common empirical bedload models of Meyer-Peter and Müller, Einstein-Brown, and Parker-Klingeman all over predict measured transport rates at Little Granite Creek. This occurs primarily because the models predict bed-material transport capacity while the majority of the measured bedload at Little Granite Creek is washload (i.e. supply limited). Using the site-calibrated hiding factor to define the critical Shields stress, both the Parker-Klingeman and Meyer-Peter Müller models predict bedload transport rates

more similar to those measured in Little Granite Creek, despite the fact that the measured load is primarily washload.

A resampling technique (bootstrapping) was used to evaluate the number of bedload samples required for model calibration. The results suggest that much of the prediction variability is eliminated with a minimum of 10 to 15 bedload samples. This estimate can be refined using cumulative frequency distributions to select the sample size based on an acceptable error from “true” values from the entire data set.

TABLE OF CONTENTS

LIST OF TABLES

LIST OF FIGURES

LIST OF SYMBOLS

The following symbols are used in this paper:

α = coefficient in power function relation between reference Shields stress and discharge;

β = Exponent in power function relation between reference Shields stress and discharge;

D_{avg} = grain size of the sediment mixture that determines bed roughness;

D_i = geometric mean particle diameter for size class *i*;

D_p = Depth of pavement layer of stream bed;

D_s = Depth of subpavement layer of stream bed;

D_{50} = median particle diameter for bed material (either pavement or subpavement);

D_{84} = 84^{th} percentile particle diameter for bed material;

d = local water depth;

exp = Parker-Klingeman (P-K) exponent;

f_i = weight fraction of bed material (pavement or subpavement) in size class *i*;

G = dimensionless bedload transport rate ratio, W^*_i / W^*_{ref} ;

GH = gauge height or water surface elevation above some local datum;

g = acceleration due to gravity;

g_s = unit bedload transport rate in the Meyer-Peter Müller formula;

k_s/k_r = ratio of grain resistance to total bed resistance in the Meyer-Peter Müller formula;

P, e, b = constants in the discharge rating curve equation;

Q = water discharge;

Q_f = Bed sub area discharge in the Meyer-Peter Müller formula;

q_{bwi} = weight bedload transport rate per unit width in size class *i*;

q_{bvi} = volumetric bedload transport rate per unit width in size class *i*;

q_{bv}^* = dimensionless volumetric unit sediment discharge in Einstein-Brown formula;

Re_* = grain Reynolds number;

R = Hydraulic radius;

S = energy slope of stream;

s_g = specific gravity of sediment particles;

u_* = shear velocity;

W^*_i = dimensionless bedload transport rate for size class *i*;

W^*_{ref} = reference dimensionless bedload transport rate, chosen to be 0.002;

ρ & ρ_s = mass density of water and mass density of sediment;

γ & γ_s = unit weight of water and unit weight of sediment;

τ = time averaged bed shear stress;

τ^*_i = Shields shear stress for particles of size class *i*;

τ^*_{ci} = critical Shields shear stress for particles of size class *i*;

τ^*_{c50} = critical Shields shear stress associated with D_{50};

τ^*_{ri} = reference Shields shear stress for particles of size class *i*;

τ^*_{r50} = reference Shields shear stress associated with D_{50} (i.e. D_{50} reference shear);

Φ_i = Shields shear stress ratio, τ^*_i / τ^*_{ri}

υ = kinematic viscosity of water

ω_0 = Rubey's (1933) clear-water fall velocity

Chapter 1: Introduction

1.1 General

Estimating bedload transport in gravel-bed rivers is notoriously problematic and often inaccurate. Methods for predicting include empirical formulas, measuring using hand-held samplers, measuring the entire load caught in slot traps or settling ponds, tracking grain movement with tracer gravels, or by constructing local sediment budgets. With the exception of the empirical formulas (in most cases), all the listed methods for developing a sediment rating curve require considerable effort and expense. The trade-off is that these methods are typically more accurate than the "off the shelf" empirical models because they are based on measurements taken at the site of interest. A potential solution to this dilemma is to use locally collected data specific to the watershed in question to calibrate an empirical formula. This typically occurs in most empirical models in the form of a characteristic sediment size and hydraulic characteristics of the stream.

What will be discussed here is using actual bedload samples (by size class) and a complete size distribution of the riverbed material to calibrate an empirical model. One such method was developed by David Dawdy and described in the literature by Bakke et al. (1999). This method makes use of the Parker-Klingeman bedload transport model, hereafter referred to as the P-K model (Parker and Klingeman, 1982). For clarity, the site-calibrated model described in Bakke et al. (1999) is referred to as the PKD model. The

transport function proposed by Parker and Klingeman contains empirical constants which vary with local hydraulic and sediment characteristics. These constants can be determined for each site by an optimization algorithm that minimizes the difference between measured bedload transport rates (model input) and predicted transport rates (model output). With such site calibration, the P-K model can be used in some cases that may be very different from those for which it was developed.

1.2 Study Objectives

The study has two primary objectives. The first is to evaluate the accuracy of prediction of the PKD model, typically using subsets of data by year of collection. The calibrated model predictions are compared to the measured data for that year as well as the entire data set. Additionally, predictions are compared to other conventional empirical bedload transport models.

The second objective is to evaluate the effects of the number of bedload samples chosen to calibrate the PKD model. The intent is to determine the variability of prediction based on subsample size and to develop a scheme to select a sample size based on an acceptable error and an exceedence probability.

Chapter 2: Theoretical Background

2.1 Initiation of Motion of Uniform Coarse Grains

A primary step in calculating bedload transport rates is determining the conditions at which individual particle sizes begin to move. This occurs when the hydraulic shear stress on the streambed exceeds some critical value required to set an individual particle in motion. Many researchers have attempted to define the shear stress required to entrain a given size particle from a bed of sediment. Most of this work has been done in laboratory flumes in order to facilitate the identification of the beginning of motion. Shields (1936) arrived at a dimensionless shear stress that incorporated the major parameters related to initiation of motion of a sediment particle. These parameters are the density of the sediment ρ_s, the grain diameter D_i, the fluid density ρ, the kinematic fluid viscosity ν, and the shear stress of the flow τ, along with the acceleration due to gravity. This dimensionless shear stress is referred to as the Shields stress and is given as

$$\tau^*_i = \tau / (\rho_s - \rho) g D_i \qquad (1)$$

This term essentially represents a ratio of the relative magnitudes of the inertial force and the gravitational force on a sediment grain acted upon by flowing water. Shields determined that τ^*_i was solely a function of the grain Reynolds number Re_*, which is defined as

$$Re_* = u_* D_i / \nu \qquad (2)$$

where $u_* = \sqrt{\tau/\rho}$ is the shear velocity.

Shields (1936) reported on a series of flume experiments conducted to determine the critical shear stresses for particles ranging from 0.36 to 3.44-mm with varying densities. For each experiment the bed was horizontal and the particles were of near uniform size. Critical Shields stress values were determined by measuring τ^* throughout a range of small transport rates and then extrapolating the relation back to a near-zero transport rate. When the dimensionless shear stress function from Equation (1) represents the condition for the threshold of motion it is referred to as the critical Shields stress τ^*_{ci}. Based upon his experiments and those of several others, Shields constructed a graph of τ^*_{ci} versus Re_* over a range of particle Reynolds numbers from about 2 to 500. The data are represented by a narrow band, below which τ^* was less than τ^*_{ci} and no significant sediment transport occurred. Above the band defined by the data, τ^* is greater than τ^*_{ci} and sediment would be in motion. The actual threshold for the beginning of sediment motion exists within the band. Later researchers modified the band to a single line, thus making use of the plot more direct (Vanoni, 1964). For grain Reynolds numbers greater than 100, the value of τ^*_{ci} approached a constant value of 0.06. Although these experiments used only uniform bed material of sand size and smaller, the results have been widely used to characterize entrainment of gravel-sized and larger particles from a non-uniform riverbed.

Miller, McCave and Komar (1977) revisited the empirical threshold curve of Shields using published data that met the following criteria: (1) experiments were performed in laboratory flumes with parallel side walls under conditions of uniform, steady flow over an initially flattened bed. Flume side wall corrections were considered

in calculating bed shear stresses; (2) particles were non-cohesive, rounded or spherical, natural or artificial grains of nearly uniform size; (3) each investigator used a consistent definition of incipient motion; and (4) sufficient data were presented to allow calculations of all required parameters.

The curve developed by Miller et al. resembles the original curve proposed by Shields but differs in several important respects. This curve expands the range of the original curve at both higher and lower grain Reynolds numbers by over three orders of magnitude. While the curve is generally the same shape, albeit longer, the slope of the curve at low values of grain Reynolds numbers has a flatter slope. Miller et al. suggested that at large values of the grain Reynolds number the fluid viscosity becomes unimportant in the threshold condition. The net result is that in the range of values of Re_* > 500, the value of τ^*_{ci} approached a constant value of 0.045, significantly less than the value of 0.06 originally suggested by Shields. Similar values have been reported by Meyer-Peter and Müller (1948) and Yalin and Karahan (1979). Consequently, critical values of the Shields stress of around 0.045 are common in engineering practice.

2.2 Initiation of Motion for Non-Uniform Coarse Grains

Critical Shields stress values reported in the literature for any given grain size within a mixture vary significantly. Part of the variation is explained by the lack of a consistent definition of the beginning of motion. The functional definitions range from a single grain in motion to 'significant transport'. Also, for sand-sized particles, the presence of bedforms can significantly affect the shear stress required to initiate motion compared to a plane bed.

Another cause for variation in the reported values of Shields stress is the effect of non-uniform bed material sizes and how this affects the beginning of motion for neighboring particles. A bed of near-uniform grains can be visualized where each grain on the surface has similar exposure to the flow. As such, any grain is equally likely to be entrained, depending on other local conditions. Beds of non-uniform materials are not so consistent as relative protrusion above/below the average bed level becomes important. Fenton and Abbott (1977) examined the effects of different degrees of particle exposure above a flume bed on initiation of particle motion. The flume bed was composed of 2.5-mm particles glued in place. A test grain was mounted on a threaded rod and inserted through the bottom of the flume and the shear stress was measured. They found that when the test grain was on top of the bed material (more exposed to the flow), the critical Shields stress was lower than that predicted for a bed of uniform grains. Conversely, when the test grain was slightly below the bed level (somewhat hidden from the flow) the critical Shields stress was much higher than that predicted for a bed of uniform grains. Even though this experiment involved only a single grain size, it showed the significant effect of particle exposure on the critical Shields stress.

Subsequent researchers (Parker et al., 1982; Andrews, 1983; Bathurst 1987; Wiberg and Smith, 1987) have found that, for a given grain size on a bed, the size distribution of the surrounding materials has an effect on the shear stress required to entrain that particle. However, common engineering practice for the selection of a critical Shields stress often does not differentiate between uniform and non-uniform beds. This may or may not be justified, depending on the particle size of interest. Andrews (1983) summarized several previous evaluations of critical Shields stress for entrainment of

gravel and cobbles from a natural riverbed. The values ranged from 0.020 to 0.25. The mean value for all the observations was approximately 0.060, the same value suggested by Shields (1936). Andrews suggests that this apparent agreement among several investigations of particle entrainment for both uniform and non-uniform beds has been used to justify neglecting the effects of particle size distribution.

Einstein's (1950) work, which forms the basis of the Parker-Klingeman transport model, considered the effects of mixed grain sizes on the transport rate of a given particle size. He developed an empirical relation that described the hiding effect that large particles have on smaller particles. This "hiding factor" is a function of the ratio of the particle diameter of interest to a characteristic particle diameter for the mixture. The characteristic particle diameter depends on the thickness of the laminar sublayer and the D_{65} (sixty fifth percentile size) of the bed material. Although this concept was not used specifically to identify critical conditions for particle entrainment, it was used to describe the reduction in fluid forces on a particle owing to the presence of larger nearby particles.

Egiazaroff (1965) also tried to account for differences in critical shear stress due to other particles in a non-uniform mixture. He derived a theoretical equation based on the forces acting on the grain during its initiation of movement. The equation took the form

$$\tau^*_{ci} = 0.1 / [\log(19D_i / D_{avg})]^2 \qquad (3)$$

Where τ^*_{ci} = the average critical Shields stress for particles of size D_i; D_{avg} = grain size of the sediment mixture that determines the roughness of the bed surface. Although Komar (1987b) describes the derivation as questionable, it still shows the history behind the

notion of relating incipient motion criteria to the effects of mixed grain sizes of the bed material.

Parker and Klingeman (1982) used the "hiding factor" concept to predict reference values of the Shields stress for a given particle size relative to the median diameter of the subsurface bed material. They developed a relationship for each size class of bedload between a dimensionless transport rate W^*_i, and the Shields stress. Reference values (rather than 'critical') of Shields stress for each size class were taken from this plot corresponding to $W^*_i = 0.002$, a small but measurable transport rate. These reference values were then plotted on a log-log scale against the ratio of D_i / D_{50}. The equation of the resulting line defines their hiding factor relationship for that site and takes the form

$$\tau^*_{ri} = \tau^*_{r50} \left(D_i / D_{50} \right)^{-exp} \tag{4}$$

$$\tau^*_{ri} = 0.0876 \left(D_i / D_{50} \right)^{-0.982} \quad \text{for Oak Creek, OR} \tag{5}$$

Where τ^*_{ri} = the reference Shields stress only slightly above the critical value for particles of size class *i*; D_i = geometric mean particle diameter for size class *i*; D_{50} = median particle diameter of the subpavement; τ^*_{r50} = the reference Shields stress associated with D_{50}; and *exp* = Parker-Klingeman exponent, as discussed below. Equation (5) was computed for ratio of particle size to median diameter in the subsurface bed material ranging from 0.045 to 4.2

Andrews (1983) and Andrews and Erman (1986) also proposed a hiding factor relationship based on field measurements that took the same basic form of Equation (4) where

$$\left(\tau^*_{ci} / \tau^*_{c50} \right) = \left(D_i / D_{50} \right)^{-exp} \tag{6}$$

Where τ^*_{c50} = the critical Shields stress associated with D_{50}; and *exp* = an exponent. The

only difference from Equation (4) is in how closely the critical value of the Shields stress relates to the reference value used by Parker and Klingeman.

Andrews (1983) computed the critical Shields stress for a given particle size from published bedload discharge measurements and shear stress values in three self-formed rivers with naturally sorted gravel and cobble beds. From the bedload data collected over a range of discharges, Andrews assumed that the calculated bed shear stress was the critical value for the largest particle in motion, as long as larger particles were still available on the riverbed. The actual dimensions of the largest particles in motion were not measured directly during the original data collection. Consequently, the geometric mean of the largest size class collected was taken to be the diameter of the maximum particle in transport. Calculated values of the Shields stress, assumed the critical value for the largest particle in motion, were plotted against the ratio of the particle size in motion and the median diameter of the subsurface material. The log-log plot yields a linear relationship for bed material sizes between 0.3 to 4.2 times the median diameter of the subsurface bed material. The average critical Shields stress was presented as

$$\tau^*_{ci} = 0.0834 \left(D_i / D_{50} \right)^{-0.872} \qquad (7)$$

where D_{50} is the median diameter of the subsurface material.

The values of τ^*_{ci} were determined to depend significantly on the size distribution of the riverbed material. As mentioned earlier, previous investigators have reported critical Shields stress values ranging from 0.25 to 0.020 for coarse sediment. Andrews' analysis suggests that virtually all of the variation is due to differences in the subsurface bed material distribution. The analysis shows that τ^*_{ci} varies almost inversely with the

particle diameter for a non-uniform bed material with the conclusion that most bed particles are entrained at nearly the same discharge.

Later work by Andrews and Nankervis (1995) and Komar (1987a) have shown that the values of τ^*_{r50} and *exp* vary between streams. For example, Andrews (1983) originally found *exp* = 0.872 relative to the subpavement but subsequent analyses have found that the exponent can approach a value of unity as the bedload size distribution approaches that of the subpavement. Komar (1987b) used field data from several sources to show that *exp* = 0.7 for conditions of unequal mobility.

Although the variations of τ^*_{r50} and *exp* between streams are rather small, the subsequent effects on predicted bedload transport rates are proportionally large. While both *exp* and τ^*_{r50} have an effect on the amount of bedload predicted, τ^*_{r50} has a greater influence on the total quantity, whereas *exp* has more of an effect on the predicted bedload size distribution (Bakke et al., 1999). Thus, determining these empirical constants for an individual location allows for a site-specific calibration of the Parker-Klingeman bedload transport function.

The value of τ^*_{ri} (or τ^*_{ci}) can be determined relative to either the pavement or subpavement particle size distribution. In theory, either approach is equally valid although the subpavement is often used since the bedload size distribution tends to more closely match that of the subpavement over time (Hollinghead, 1971; Andrews and Parker, 1987). Also, the subpavement size distribution is often easier to reliably characterize due to the smaller maximum particle sizes. Andrews (1983) evaluated both surface and subsurface distributions in predicting initiation of motion and concluded that the subsurface D_{50} is more closely correlated with critical conditions for motion.

2.3 Parker-Klingeman Bedload Transport Model

The P-K bedload transport model (Parker and Klingeman, 1982) was developed from data collected by Milhous (1973) at Oak Creek, Oregon. A key assumption within the model is that the riverbed develops a coarsened surface layer (pavement) that is present at all discharges. This pavement layer then regulates the exchange between the bed material and the bedload. The model is clearly described by Bakke and others (1999) and summarized below.

The site-specific hiding factor relationship (Equation 4) is used in the P-K model as part of the normalized Shields stress, Φ_i, which Parker and Klingeman define as

$$\Phi_i = \tau^*_i / \tau^*_{ri} \quad (8)$$

Where τ^*_i is the Shields stress for a particle of size class *i*, defined as

$$\tau^*_i = \tau / (\rho_s - \rho)\, g\, D_i \quad (1)$$

and

$\tau = \gamma dS$ = local bed shear stress
ρ_s = mass density of the sediment
ρ = mass density of water
d = depth of water at location of interest
S = energy slope of the river
D_i = diameter of sediment particle of interest

Parker and Klingeman (1982) then defined a dimensionless bedload transport rate ratio, G, as

$$G = W^*_i / W^*_{ref} \quad (9)$$

Where W^*_{ref} = a reference dimensionless bedload transport rate, chosen by Parker and Klingeman to represent a small but measurable transport rate of 0.002. Also, W^*_i is the dimensionless bedload transport rate for size class *i* defined as

$$W^*_i = (s_g\text{-}1)\, q_{bvi} / (f_i\, g^{1/2}\, (dS)^{3/2}) \quad (10)$$

where

q_{bvi} = volumetric bedload transport rate per unit width in size class *i*;
s_g = specific gravity of sediment particles;
f_i = fraction of bed material (pavement or subpavement) in size class *i*.

These definitions facilitated a collapse of the measured data onto a single curve, which is fitted to the following bedload transport function

$$G = 5.6 \times 10^3\, (1 - 0.853/\, \Phi_i\,)^{\,4.5} \quad (11)$$

This relationship, along with that for the hiding factor and the definitions of Φ_i and W^*_i, constitute the P-K bedload transport model (Parker and Klingeman, 1982). By rearranging the equations above, the weight sediment transport rate per unit width in size class *i* is determined for each point in the channel cross section as

$$q_{bwi} = (f_i\, g^{1/2}\, (d\, S)^{3/2})\, W^*_{ref}\, G\, \gamma\, s_g / (s_g - 1) \quad (12)$$

Calculated unit transport rates are then multiplied by their width increment and summed across the cross section to yield a total bedload transport rate by size class. Though not obvious from the final form, Equation (12) contains the hiding factor relationship discussed previously. This is what allows site calibration of the P-K model to local conditions.

Sample bedload calculations using the Parker-Klingeman model are included in Appendix A.

Chapter 3: Study Site

3.1 General

Little Granite Creek is a 55 square kilometer watershed in SW Wyoming. The study site is located near the mouth of Little Granite Creek, just prior to its confluence with Granite Creek, a tributary to the Hoback River. The study site is at approximately 1948 meters in elevation, with the highest point in the basin over 3,400 meters in elevation. The terrain is generally steep and forested with areas of ridge top meadows. The dominant vegetation consists primarily of spruce and fir on north and east aspects, and meadows with aspen and sagebrush along with lodge pole pine on south and west aspects. The geology of the area is primarily sandstones reworked by glaciation, with local areas of granite. The dominant soils in the forested areas are fine sandy loams and those in the open areas tend to be silty loams or silty clay loams.

The streamflow regime is dominated by snowmelt, with a peak typically occurring in late May or early June. The Idaho district of the U.S. Geological Survey operated a stream gaging station at the site from 1981 through 1992 (station number 13019438). The hydrograph of the mean daily discharges for the period of record is shown in Figure 4. The stage discharge data for the sediment cross section are tabulated in Table 6 in Appendix A. Other relevant hydrologic characteristics at the gage site as summarized by Emmett (1998 and 1999) are listed below:

Bankfull discharge	229	cfs
Bankfull discharge return period	1.6	years
Bankfull width	23.6	feet
Bankfull depth	1.8	feet
Bankfull velocity	5.5	ft/sec
Average annual streamflow	29.5	ft^3/sec
Depth of average annual runoff	19.0	inches
Average annual bedload	17.2	tons/sq.mi

The water surface slope is used to approximate the energy slope. The US Forest Service Rocky Mountain Research Station measured this value for Little Granite Creek in 1997 on three occasions. The measured slope at the sediment sampling site varied from 0.018 to 0.020 for flows near bankfull to approximately 150% of bankfull.

A longitudinal profile of the study site and cross sections at the gage location and the sediment sampling location are included in Appendix C.

3.2 Hydraulics

Stage-discharge information for the period of record for the Little Granite Creek gage was retrieved from the USGS. A mathematical relationship was then developed that took the form

$$Q = P(GH - e)^b \quad (13)$$

Where Q = water discharge in cubic feet per second, GH = gage height of water surface in feet, and P, e, and b are constants determined by methods outlined by Rantz (1982). Using the rating curve at the gage site presented a problem since the stream gage cross section and reach gradient are quite different from the cross section and reach gradient at the sediment sampling site. In other words, the stage-discharge relationship for the gage location did not accurately reflect the stage-discharge relation (and shear stress) at the sediment sampling location. Using several known stage-discharge data pairs at the

sediment cross section, a new rating curve was reconstructed for the sediment sampling cross section. The final rating curve was

$$Q = 37(GH-96.10)^{2.36} \quad (14)$$

One assumption inherent in the multi-year analysis is that the cross section has remained relatively unchanged over time. Annual changes in the cross section would affect the relationship between discharge and shear, and subsequently the optimization process within the PKD model (see Chapter V). A cursory review of the cross sectional data available for Little Granite showed only minor changes over time. Cross sectional changes are not expected to be a significant source of error in this analysis.

Flow duration information was also obtained from the Idaho District of the USGS for the period of record at the Little Granite Creek gage.

3.3 Bed Material Measurements

The bed material distributions for Little Granite Creek are very coarse, the distributions of which are shown in Figure 1 and Appendix B. Common percentiles for the composite subpavement and pavement bed material distributions and the surface pebble count are summarized in Table 1. Also reported are the gradations of the sediment mixtures, defined as the square root of the ratio of the D_{84} and D_{16} (Julien, 1995).

Table 1. Bed material sampling percentile summary for Little Granite Creek.

Sample	Method	D_{16}	D_{50}	D_{84}	$(D_{84}/D_{16})^{1/2}$
Subpavement	Volumetric	2.8	20.8	97	5.9
Pavement	Volumetric	23.0	107	209	3.0
Pavement	Pebble Count	17.8	74	181	3.2

Volumetric samples of the riverbed pavement and subpavement were sampled and sieved during the fall of 1999. The intent was to characterize the bed material sediment in the vicinity of the cross section used for bedload sampling. Bed material sampling was

done just upstream of the bedload sampling cross section, but still within the same hydraulic control. Sample locations were chosen that were representative of the reach being evaluated, typically a riffle or run. Pools, deposits behind boulders, etc. were avoided in the sampling layout. Samples of both the pavement and subpavement were collected using a three-sided plywood shield instead of a barrel sampler.

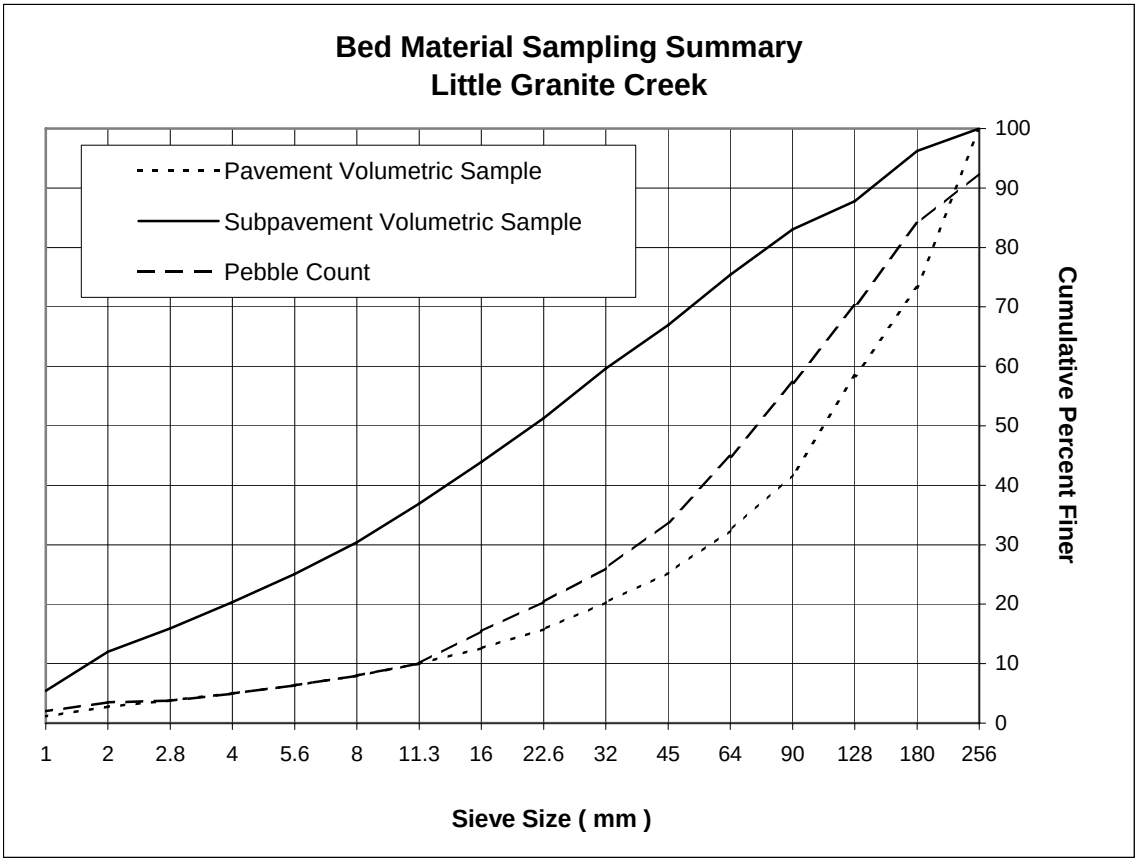

Figure 1. Cumulative distributions of bed material samples.

The extent of the pavement layer was defined by the largest vertically oriented depth of any exposed surface particle within the sampling area. This is referred to as the embedded depth. See Figure 2. Once the pavement was removed, this same depth was used to define the limit of the subpavement sample.

Usually the volumes of pavement and subpavement collected at a given sample site were not equal. This occurred for a couple of reasons. First of all, the submerged bed material will not stand vertically. Consequently, the sampling hole became cone-shaped as it became deeper, thus reducing the volume of the subpavement sample relative to the pavement. Secondly, the pavement depth was measured from the plane of embeddedness (Figure 2), not the top of the large surface particles. Since these large particles extend past this plane, the volume of the pavement sample was larger than the subpavement by an amount proportional to the volume of pavement particles which extend beyond that plane.

Figure 2. Determination of sampling depth for pavement and subpavement. D_p and D_s are the depth of the pavement and subpavement, respectively.

To compensate for differing sample sizes, the distributions were evaluated as proportions by weight. Individual samples were composited by both weight and proportion. Because of the variations in embedded depths, there were slight differences in the distributions composited by weight and by proportion for Little Granite Creek. Bed material measurements are summarized in the following table. Size distributions for each individual bed material sample are shown in Appendix B.

Since the stream reach had very coarse bed material, selecting a sample size large enough to avoid bias was a concern. The arbitrary presence or absence of large particles

in bed material samples not only affects the total sample mass, but it will affect the particle size distribution as well. To avoid sampling bias from the arbitrary presence/absence of the largest particles, sample masses must be large enough to representatively sample all size classes present.

Table 2. Pavement and subpavement sampling summary.

Bed Material Sampling Summary			
Location	Sample ID	Embedded Depth (cm)	Sample Weight (kg)
Little Granite Creek	1-Pavement	10	88.7
	2-Pavement	13	141.2
	3-Pavement	7	68.7
	4-Pavement	9	74.8
	5-Pavement	13	135.9
	TOTAL		**509.3**
Little Granite Creek	1-Subpavement	10	44.6
	2-Subpavement	13	73.4
	3-Subpavement	7	52.0
	4-Subpavement	9	46.9
	5-Subpavement	13	67.0
	TOTAL		**283.9**

In the literature, the necessary sample mass is usually depicted as a function of a bed material particle size D, where D is a characteristic large particle size percentile, usually the D_{max} or D_{95} (Bunte and Abt, 1999). Church and others (1987) empirically determined that the mass of the largest particle in the sample should not exceed about 0.1% of the total sample mass. This translates into a minimum sample mass of 1000 times the mass of the D_{max} particle size and yields very large sample sizes for material greater than 32-mm. Consequently, they modified the mass criteria as the maximum particle size increased. For coarse gravel with D_{max} between 32 and 128-mm, the largest particle may account for one percent of the total sample mass. Similarly, for D_{max} greater than 128-mm the largest particle may account for up to five percent of the total sample mass. Figure 3.9 in Church et al. (1987) summarizes these criteria as a plot of log(sample

size in kg) versus log(b-axis of largest stone in mm). This plot may be summarized with the following formulas.

$$D_{max}\,(kg) / \text{Sample mass (kg)} < 0.001 \qquad \text{for } D_{max} < 32\text{-mm} \qquad (15)$$

$$D_{max}\,(kg) / \text{Sample mass (kg)} < 0.01 \qquad \text{for } 32 < D_{max} < 128\text{-mm} \qquad (16)$$

$$D_{max}\,(kg) / \text{Sample mass (kg)} < 0.05 \qquad \text{for } D_{max} > 128\text{-mm} \qquad (17)$$

At Little Granite Creek, the largest particles in both the subpavement and pavement samples were 128-mm or larger. Thus the "five percent" criterion was applied in determining the sample size. The largest subpavement particle sampled was 9,980 grams, which accounted for 3.5 percent of the total sample size. The largest pavement particle was 30,230 grams, which constituted 5.9 percent of the total sample size. So even with a sample size of nearly 510 kilograms, the maximum size particle in the pavement still slightly exceeds the sample size criterion.

For subsequent model calibration and other calculations, only the subpavement distribution is used. For the subpavement, the largest particles were well represented in the samples and no individual particles were large enough to create significant bias in the distributions based on the criteria by Church et al. (1987).

A 400-sample pebble count (Wolman, 1954) was also done to describe the pavement material. A sampling grid was used to more objectively select particles for measurement. The grid consisted of a 600-mm square frame with elastic bands forming a matrix of 3 rows by 3 columns. The intersections of these bands form four "crosshairs" that identify the particle to be selected. The frame was moved at equal increments across the stream and placed diagonally for sampling at each sample location. This was repeated

for four cross sections within the sampling reach to attain the minimum of 400 samples. The data are shown in Appendix D and summarized previously in Table 1 and Figure 1.

3.4 Bedload Measurements

For this analysis, bedload is defined as that part of the river's total sediment load that is moving on, or near, the bed by rolling, saltating or sliding. Bedload samples (summarized by full phi size class) were collected at Little Granite Creek from 1982 to 1993, and again in 1997 using a 76-mm (3-inch) Helley-Smith hand held sampler. With the exception of 1997, all data were collected by the Idaho District of the U.S. Geological Survey. The 1997 data were collected by the US Forest Service Rocky Mountain Research Station. Bedload measurements cover a range of stream discharges from approximately 10 to 180 percent of bankfull flow.

The bedload sampling scheme generally consisted of two transects of 20 verticals for 30 seconds each. The first three years of data have only one transect for each measurement, so subsequent years typically show each transect as a separate measurement. Dual transects were composited back into a single measurement for this analysis, giving a total sample size of 133 measurements. The data are analyzed in annual groups, except for data year 1992 since this consisted of only three measurements at very low discharges. The data set from 1982 – 1993 had several measurements above bankfull discharge (estimated at 229 cfs) but primarily characterized transport rates at lower discharges. The 1997 data are comprised of measurements almost entirely above bankfull discharge. Bedload data are summarized in Appendix E.

A noteworthy feature of the bedload data set is that it was collected entirely with a 76-mm (3-inch) Helley-Smith sampler by either wading or via a constructed footbridge.

Both the pavement and subpavement have a large portion of their distribution that would not readily fit into the sampler. This is likely mitigated by the small probability of catching a large sized particle within the relatively short sampling period and the limited width being sampled for each vertical. However, anecdotal accounts indicate that much of the bed of Little Granite Creek was mobile at discharges around two hundred percent of bankfull.

The sediment rating curves for all data years, including the least squares regression line of all the data, are shown in Figure 3. Considerable variability exists among the yearly rating curves; some fall below the overall regression line and several lie above.

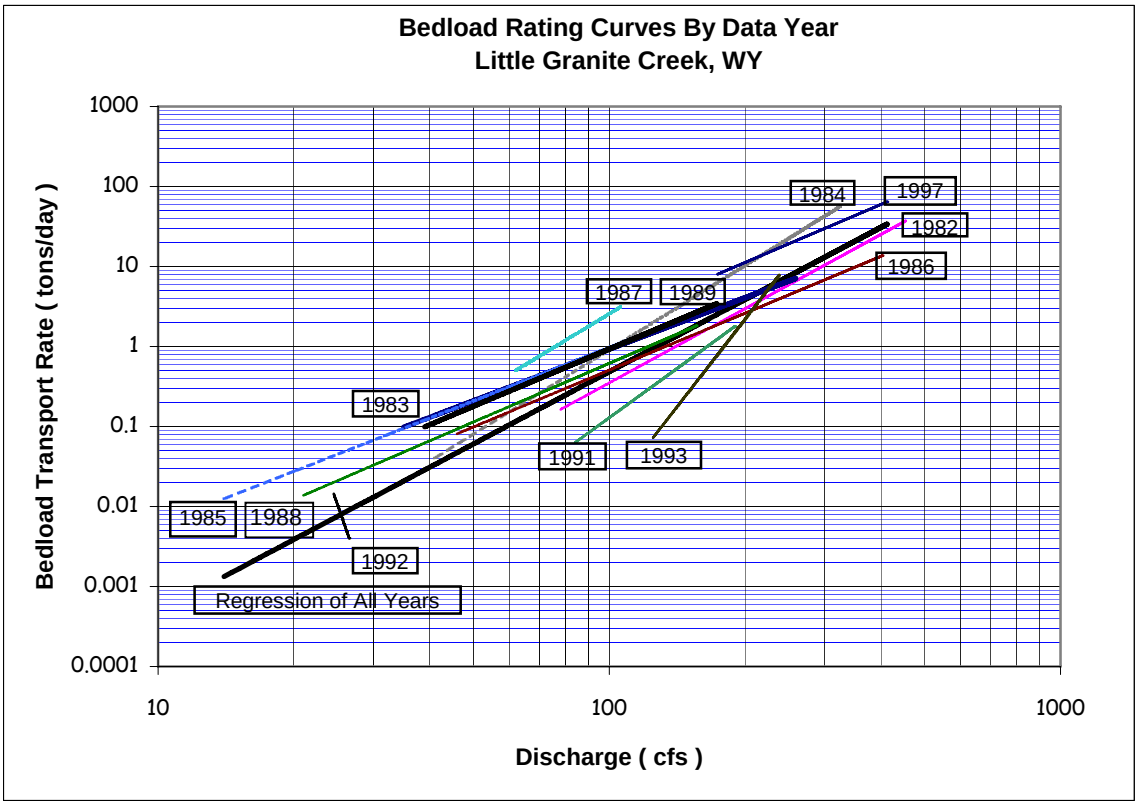

Figure 3. Annual measured bedload rating curves for Little Granite Creek.

The variability inherent in bedload discharge measurements is logically attributed to such factors as sampling variability, changes in sediment supply with subsequent changes is bed material gradation, relative "packing" of the bed material, and even the passing of bedload waves. Unfortunately, much of this information is not available for Little Granite Creek.

Sampling variability is not likely a major cause of the annual variation in the rating curves. All data for years prior to 1997 were collected by the Idaho District of the USGS. Essentially the same crew used the same methodology year after year. The 1997 data were collected by a different crew but the sampling protocol was the same.

There are no data for landslide volumes or other large sediment inputs for Little Granite Creek to evaluate changes in sediment supply. Similarly, there is no data set that characterizes changes in the bed material distribution or packing over time.

Reid and others (1985) suggest that the condition of the streambed will account for a large variation in transport rates at the same discharge. Long periods of inactivity encourage the channel bed to consolidate and produce lower bedload transport rates than those beds that were recently disturbed. Conversely, high flows result in a disruption of the streambed so that the bed material is comparatively loose and offers less resistance to entrainment.

To examine these conditions in Little Granite Creek, mean daily flows were plotted for the period of record in Figure 4. In general, annual bedload rating curves (See Figure 3) for which the *previous* season had mean daily flows in excess of bankfull discharge typically plotted above the overall regression line. For example, high stream flows that occurred in 1982-1984, 1986 and 1996 were followed by years that had higher

than average bedload transport rates for a given discharge. For this discussion, 'average' is characterized by the least squares regression line through the entire data set. Antecedent flow conditions for data year 1997 were determined from the gage on the Gros Ventre River at Zenith, WY (station number 13015000).

Conversely, bedload sampling years 1986, 1988, 1991, and 1993 were all preceded by years where the largest mean daily flows were less than bankfull discharge. This generally resulted in rating curves that predicted lower than average bedload transport rates. This presumably occurred because the bed was coarser and more tightly armored in the absence of bed-disturbing discharges or increased sediment supply from the previous year.

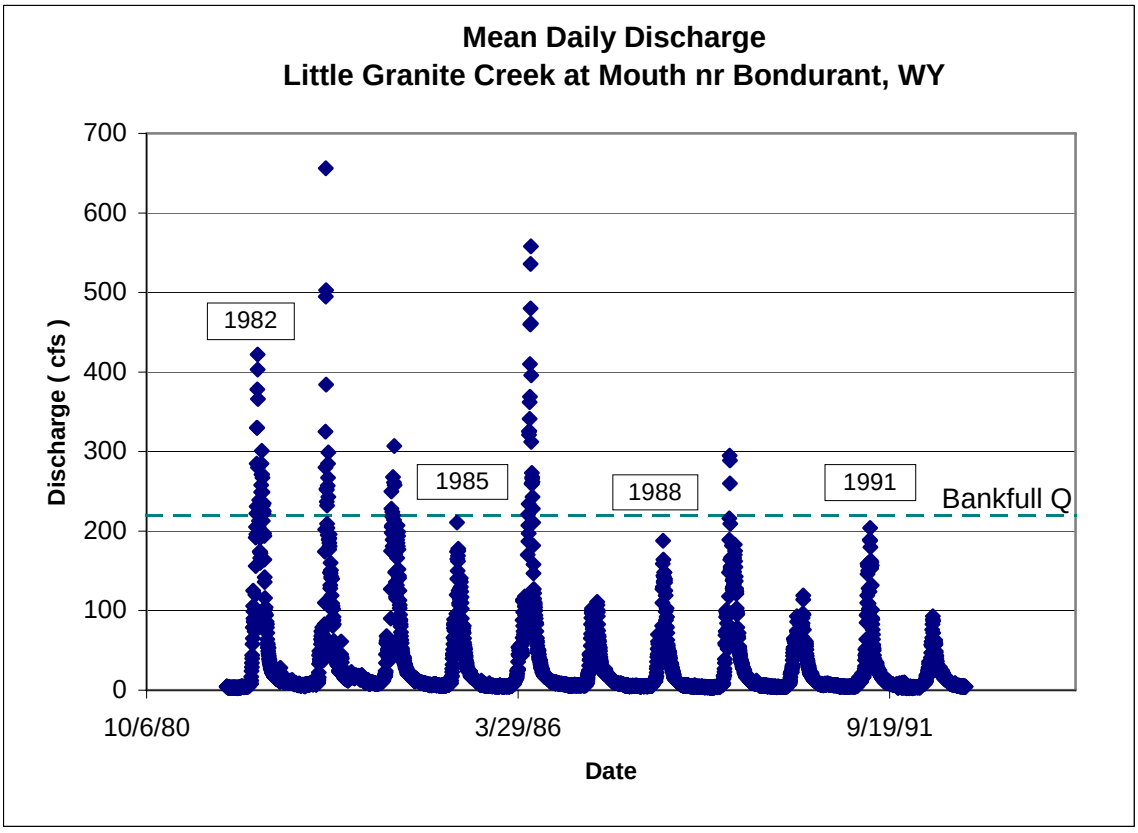

Figure 4. Mean daily flows for the period of record at Little Granite Creek.

Figure 5 gives additional evidence of this segregation of data based on antecedent stream flows. The bedload data set for Little Granite is split into two groups. One group is bedload measurements that had mean daily flows greater than bankfull discharge the *prior* year. The second group of data points consists of bedload measurements that had mean daily flows less than bankfull discharge the prior year. Data year 1982 is not included in this plot since no data were readily available for antecedent flows. The center portion of the data set, on either side of the least squares regression line, has an overlap of the two groups. However, the highest transport rates at a given discharge are generally associated with high flow antecedent conditions. Similarly, the lowest transport rates at a given discharge are generally associated with low flow antecedent conditions.

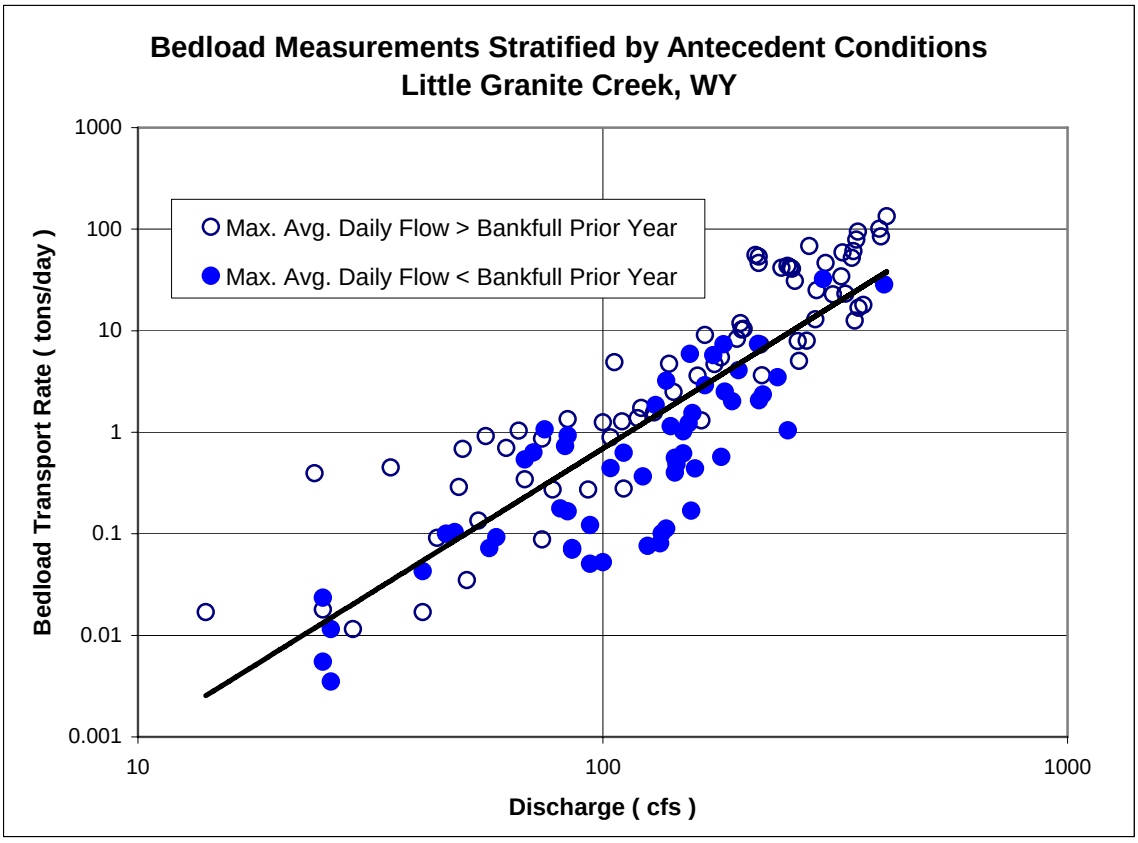

Figure 5. Stratification of Little Granite Creek bedload samples by antecedent flows.

The physical meaning of Figure 5 becomes more clear when the measured bedload is viewed as separate components based on either supply or transport capacity limitations. The component of the bedload that is determined primarily by supply limitations from upstream sources is considered washload. Washload is characterized by fine particles with low abundance in the riverbed (Julien, 1995). Bed-material load, on the other hand, is the capacity limited portion of the bedload that is hydraulically derived from disturbing the pavement layer. The rate of bed-material load in transport is determined by the capacity of the flow to move the particle sizes commonly found in the bed. The variability of the transport rates in Figure 5 with antecedent conditions (i.e., supply) suggests that a significant portion of the bedload in Little Granite Creek is washload. This notion is examined in more detail in Chapter IV with an effort to quantify the grain sizes that make up washload in Little Granite Creek.

The other implication from Figure 5 is that basing a bedload rating curve on only one or two years of data may be an inaccurate representation of the system. If washload is a significant component of the bedload, multiple years of sampling with different antecedent conditions is likely necessary to capture the potential range of bedload transport rates possible at a given discharge. This is particularly important when selecting bedload samples to calibrate the PKD model.

Chapter 4: Bedload Predictions With Traditional Models

4.1 Meyer-Peter and Müller

Meyer-Peter and Müller (1948) developed a bedload transport function for gravel-sized material from flume data. The experiments to develop the equations were done with effective diameter of sediments between 6.4 and 30 mm, and specific gravity for sediments from 1.25 to over 4. The formula is considered applicable to coarse sediments with little suspended load (Chang, 1998). The original equation took the form

$$(k_s/k_r)^{3/2} (Q_f/Q) (\gamma/(\gamma_s-\gamma)) (RS/D_i) = 0.047 + 0.25 (\gamma/g)^{1/3} (g_s^{2/3}/(\gamma_s-\gamma)D_i)) \qquad (18)$$

where

D_i = the geometric mean grain size diameter
S = slope
R = hydraulic radius
k_s/k_r = ratio of grain resistance to total bed resistance
Q_f/Q = ratio of the bed sub-area discharge to the total discharge
g_s = bedload transport rate [dimensions of M/T^3]
γ_s and γ = unit weights of the sediment and water, respectively

For plane bed conditions $k_s/k_r = 1$ and for channels with width/depth ratios greater than ten to fifteen, $Q_f/Q = 1$. Making the above approximations for gravel-sized materials, Equation (18) reduces to

$$g_s = \frac{8[(\rho_s - \rho)gD_i]^{1.5}}{\rho^{0.5}} \left[\frac{\gamma RS}{(\rho_s - \rho)gD_i} - 0.047\right]^{1.5} \qquad (19)$$

where

ρ = mass density of water
ρ_s = mass density of sediment

At the point where the bedload transport, g_s, is zero, equation (19) indicates that the critical Shields stress was taken to be 0.047. Julien (1995) provides a version of this equation based on the work of Chien (1956) for the unit volumetric bedload transport rate, which takes the form

$$q_{bvi} = 8 (\tau^* - \tau^*_c)^{3/2} [(s_g-1) g D_i^3]^{1/2} \quad (20)$$

Calculations using Equation (20) and the hydraulic data from Little Granite Creek were performed to predict bedload transport rates. Calculations were done in small width increments across the channel so that changes in bed configuration were represented by changes in shear, rather than using an average depth or hydraulic radius. Transport rates were computed using the median diameter of both the pavement and subpavement bed material. The value of τ^*_c was initially set to 0.047, the value first suggested by Meyer-Peter and Müller. The predicted total transport rates are shown in Figure 6, along with the measured data for Little Granite Creek.

Sample bedload calculations using the Meyer-Peter and Müller equation are shown in Appendix A.

4.2 Einstein-Brown

Einstein (1942, 1950) conducted extensive work in sediment transport based on fluid mechanics and probability using data from both flume studies and field measurements. Although the original research was tested using sand sized material, Einstein (1950) described the bedload function as being applicable to coarse sediment.

This original work has served as the basis for much further research, including what is referred to as the Einstein-Brown equation (Brown, 1950). This formulation is unique in that it does not use a critical shear stress or critical dimensionless shear stress.

Julien (1995) summarizes the Einstein-Brown equation, which gives the contact sediment discharge in volume of sediment per unit width and time as

$$q_{bvi} = K\, q_{bv}^{*} \qquad (21)$$

where

q_{bv}^{*} = dimensionless volumetric unit sediment discharge
$K = \omega_0 D_i = [(s_g\text{-}1)\, g\, D_i^3]^{1/2}\ \{[2/3 + 36\upsilon^2 / ((s_g\text{ -}1)\, g\, D_i^3)]^{1/2} - [36\, \upsilon^2 / ((s_g\text{ -}1)\, g\, D_i^3)]^{1/2}\}$
ω_0 = Rubey's (1933) clear-water fall velocity
υ = kinematic viscosity of water
D_i = sediment particle size of concern
s_g = specific gravity of sediment

The parameter definitions above require a consistent set of units. The value of the dimensionless volumetric unit sediment discharge is calculated in one of three ways, depending on the value of the Shields stress τ^*, as

$$q_{bv}^{*} = 2.15\, e^{-0.391 / \tau^*} \qquad \text{when } \tau^* < 0.18 \qquad (22)$$

$$q_{bv}^{*} = 40\, \tau^{*3} \qquad \text{when } 0.18 < \tau^* < 0.52 \qquad (23)$$

$$q_{bv}^{*} = 15\, \tau^{*1.5} \qquad \text{when } \tau^* > 0.52 \qquad (24)$$

Calculations were again done with the same small width increments across the channel. Transport rates were computed by full phi size class by using the geometric mean particle diameter as D_i. These transport rates were scaled by f_i, the proportion of each size class found in either the pavement or subpavement particle size distribution. Transport rates by size class were summed to yield total transport rates. The predicted bedload transport rates using Einstein-Brown, along with the measured data, are shown in Figure 6.

Sample bedload calculations using the Einstein-Brown equations are also shown in Appendix A.

4.3 Parker-Klingeman

The Parker and Klingeman (1982) bedload transport equations, described in detail in Chapter II, are also used to predict bedload transport in Little Granite Creek. This method does account for the hiding factor but uses the values from Oak Creek, OR, which takes the form

$$\tau^*_r = 0.0876 \, (D_i / D_{50})^{-0.982} \qquad (5)$$

This formulation is relative to the subsurface bed material and was developed specifically for gravel-sized material. The predicted bedload transport rates using Parker-Klingeman, along with the measured data, are shown in Figure 6.

Sample bedload calculations using the Parker-Klingeman equation are also shown in Appendix A.

4.4 Bedload Model Prediction Summary

The bedload transport models by Meyer-Peter and Müller (1948), Einstein via the Einstein-Brown equation (Brown, 1950), and Parker and Klingeman (1982) all grossly over predict the measured transport rates at Little Granite Creek. This is not surprising since Little Granite Creek has a steeper gradient and coarser bed material than the conditions under which the other models were developed. Also, these predictive equations are for bed-material load and assume an unlimited supply of material for transport. In reality, the coarse pavement layer at Little Granite Creek limits the availability of finer grained particles until that layer is disturbed. Consequently, while the equations are predicting bed-material load with unlimited supply, the bedload in Little Granite appears to be largely supply limited (washload).

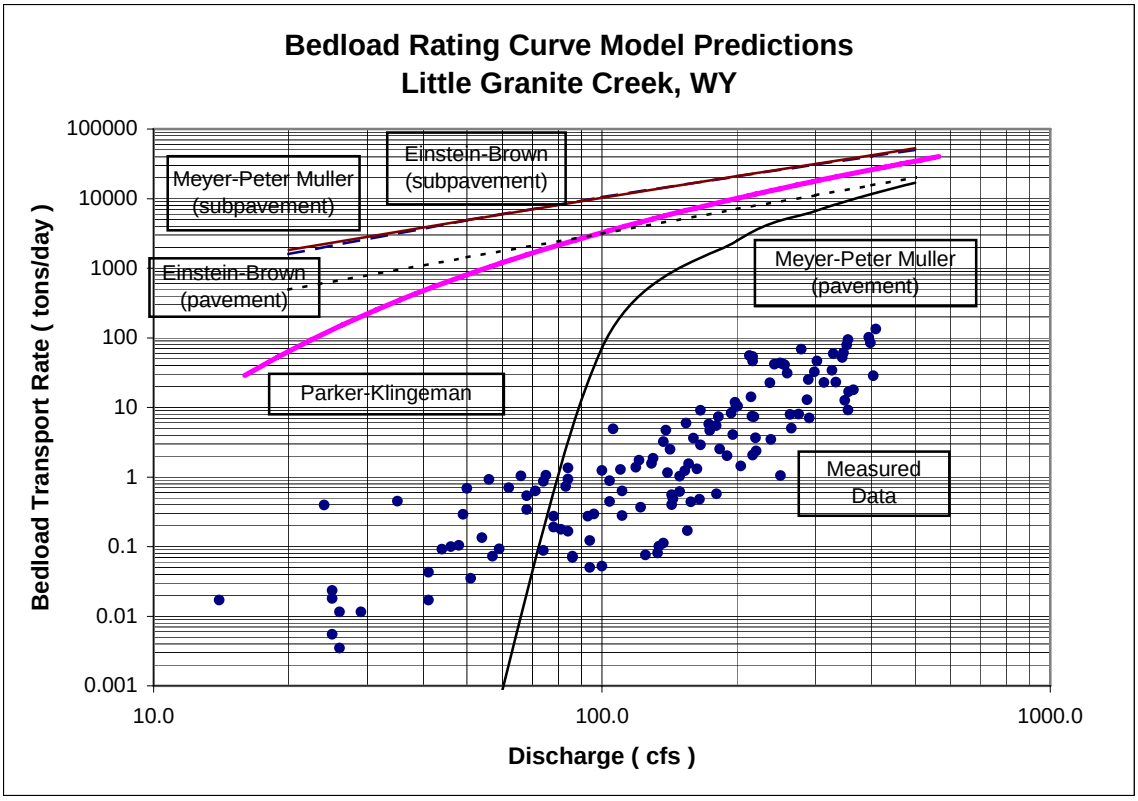

Figure 6. Bedload predictions with conventional models.

Although washload is often associated with very fine particles such as silts and clays, the size range changes based on the distribution of the bed material. Einstein (1950) and Julien (1995) delineate washload as particles sizes $D_i < D_{10}$, where D_{10} is the tenth percentile particle size on the bed surface. Figure 7 shows the distribution of the bed material and the average size distributions of the measured bedload at discharges of 25, 200 and 350 cfs. Based on the pavement D_{10} of approximately 11 mm, all of the measured bedload at 25 cfs would be considered washload. Similarly, 65–70 percent of the measured bedload at discharges of 200 and 350 cfs would be considered washload.

Another method for delineating washload is by visually examining curves of the sediment supply and the transport capacity. The point at which the sediment supply and

the sediment transport capacity curves intersect separates washload and bed-material load (Julien, 1995).

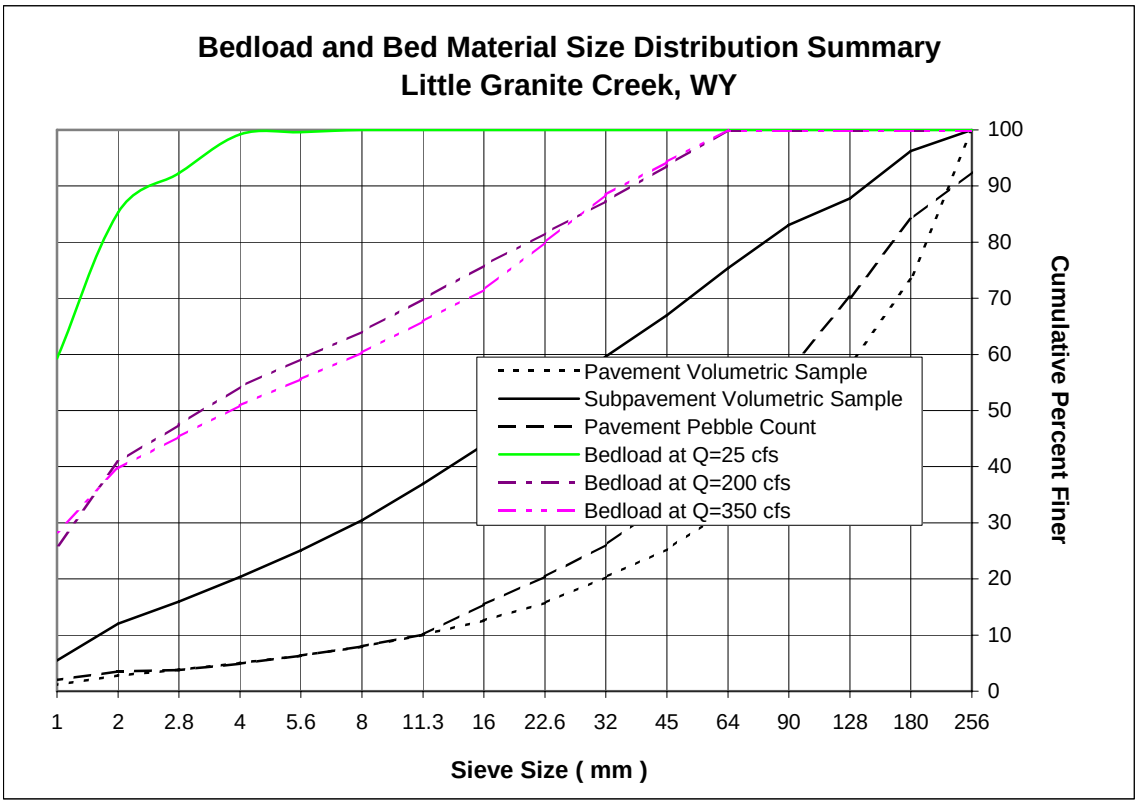

Figure 7. Bed material and bedload size distribution summary.

The sediment transport capacity is calculated for each grain size (assuming uniform grains) using the Meyer-Peter Müller model with the default value of $\tau^*_c = 0.047$. Bed-material transport capacity rates are plotted against grain size in Figure 8 for stream discharges of 20 and 250 cfs. Around a discharge of 250 cfs, particles similar in size to the pavement D_{50} are at incipient motion. At this point, finer grained material from the subpavement would be exposed and available for transport. The availability of this fine-grained material would be indistinguishable from sources of washload. Consequently, discharges above 250 cfs are not used in this graphical delineation of washload and bed-material load.

The rate of sediment supply to the stream is more problematic to quantify, particularly by particle size. Since the intent here is to roughly quantify the particle sizes associated with washload, a simplifying assumption is made. That is, the rate of sediment supply to the stream is approximated by the measured bedload transport rates. Also, rather than evaluating the supply by size fraction (which have limited data), the sum of all size classes is used to represent the supply. This approximation is not expected to result in significant error since the slopes of the transport capacity curves are so steep in the area of concern that an order of magnitude change in supply results in a modest change in grain size in Figure 8.

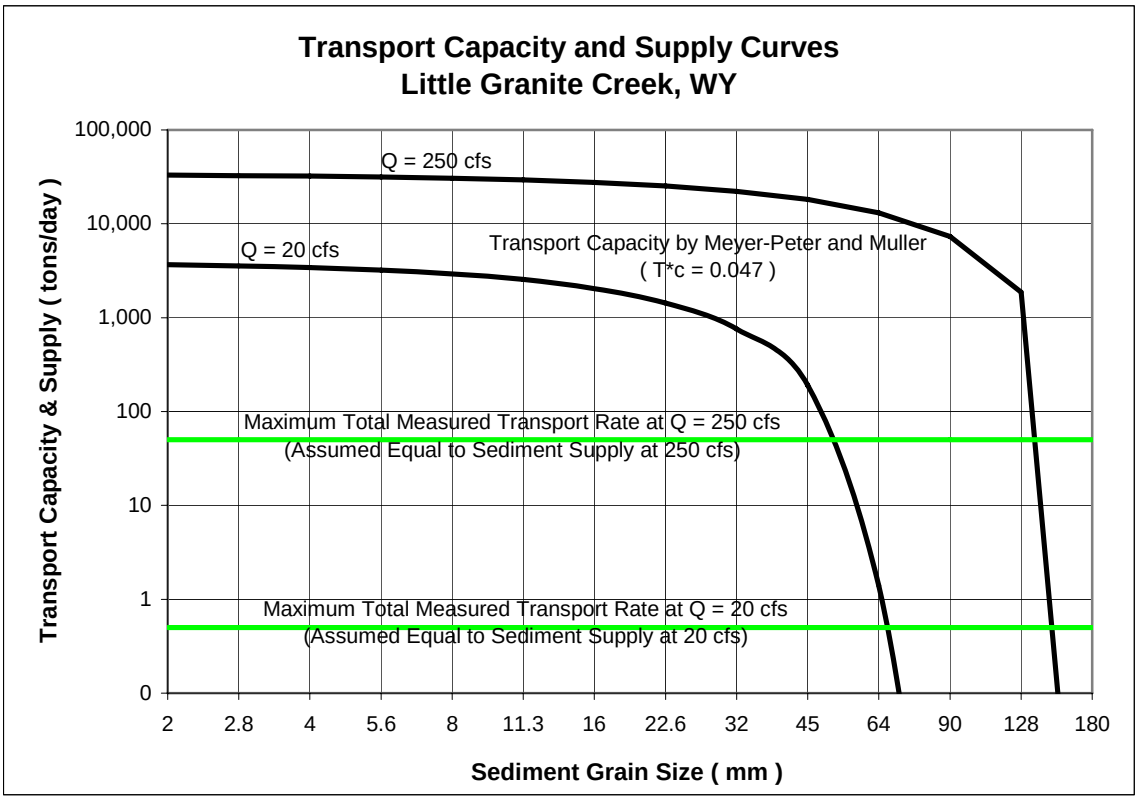

Figure 8. Transport capacity and supply curves for Little Granite Creek.

At a discharge of 250 cfs, the measured bedload transport rate was as high as 50 tons per day, which intersects the transport capacity curve between the 128 and 180-mm

particle sizes. This suggests that bedload finer than approximately 128-mm might be considered washload. Similarly, for a measured transport rate of 0.5 tons/day at 20 cfs, the intersection with the transport capacity curve is between 45 and 64-mm. At a discharge of 20 cfs, washload might include grain sizes less than 45-mm.

Based on these two methodologies, the bedload for Little Granite Creek can be roughly partitioned as follows:

D_s < 11-mm	washload
11-mm < D_s < 128-mm	washload or bed-material load
D_s > 128-mm	bed-material load

This delineation suggests that most of the measured bedload at Little Granite Creek could be classified as washload. As such, transport rates would be governed primarily by sediment supply rather than the transport capacity of the stream and could not be accurately predicted by the conventional bed-material transport models.

Chapter 5: Site-Calibrated (PKD) Model

5.1 Model Operation

The PKD model is an adaptation of the Parker and Klingeman (1982) bedload transport equations in which site-specific values in the hiding factor relationship are used. The entire optimization and prediction model consists of two FORTRAN programs. SEDCOMP is the first program that will optimize the two parameters in the hiding factor equation (reference Shields shear stress associated with D_{50} and exponent) by incrementally adjusting each of those two parameters until the predicted bedload in the Parker-Klingeman equation is equal to the measured bedload used in the input file. The optimum values of the D_{50} reference shear and exponent are those values that produce the minimum squared error (by total and size class) between the measured and predicted bedload transport rates. See Section 5.3 for a detailed description of the parameter optimization process.

The second program is FLOWDUR, which uses the previously optimized parameters to predict bedload transport rates for a range of discharges that are defined in a user supplied flow duration table. FLOWDUR also computes annual loads, distribution of bedload by size class, and thresholds for particle motion.

5.2 Model inputs

The data requirements for the model to run consist of a cross section and stage-discharge rating curve, bed material size distribution (subpavement in this analysis),

bedload samples reported by size class, local energy slope and a flow duration curve. Since energy slope is a key component of shear stress, the user of the SEDCOMP has the option to limit the energy slope to that related only to grain resistance, not form resistance. The resistance parameter for grain resistance is calculated, based on the surface material D_{50} or D_{84}, with a modification of the Limerinos (1970) equation as adapted by Burkham and Dawdy (1976). From this parameter, the energy slope can be back calculated from either the Manning or the Darcy-Weisbach equation. This adjustment was initially used at Little Granite Creek but created more scatter in the optimization process than by using the single measured slope value. This slope limitation was not used in the optimization process.

5.3 Parameter Optimization Process

5.3.1 Model Algorithm

The algorithm that the SEDCOMP model follows is described below, and summarized in the flow chart shown in Figure 9. Sample calculations of the optimization process are shown in Appendix F. SEDCOMP sample input files and definitions of terms are shown in Appendix G.

For a given bedload sample at a given discharge, or a group of samples at the average discharge, initial values of the hiding factor parameters (τ^*_{r50} and *exp*) are assumed. The cross section is then broken into verticals based on the input file elevation/offset points.

For each vertical in the cross section, the depth is calculated from the rating curve. From the depth and known energy slope the bed shear stress is calculated as

$$\tau = \gamma \, d \, S \qquad (25)$$

For the geometric mean grain size of each size class the Shields stress τ^*_i, is calculated as

$$\tau^*_i = \tau / (\rho_s - \rho)\, g\, D_i \qquad (1)$$

Since values of reference shear (τ^*_{r50}) and P-K exponent (*exp*) are known, based on initial values and set increments, the reference Shields stress relative to the subpavement D_{50} for each particle size is calculated as

$$\tau^*_{ri} = \tau^*_{r50}\, (D_i/D_{50})^{-exp} \qquad (4)$$

The Shields stress ratio is calculated for each size class as

$$\Phi_i = \tau^*_i / \tau^*_{ri} \qquad (8)$$

The unit bedload transport rates by weight (q_{bwi}) for each vertical are then calculated with Equations (11) and (12).

Repeat this process for all other size classes.

Repeat this process for all other verticals (flow depths).

The total transport rate is calculated for each size class by summing q_{bwi} across all the verticals in the cross section. All transport rates by size class are summed to yield the total transport rate. The calculated transport rates are compared to the measured rates and the average squared error is determined for the prediction. At this point, for the τ^*_{r50} being used, a measured and calculated transport rate and squared error are known. The value of τ^*_{r50} is incremented upward, still at the same *exp*, and the calculations repeated. Once τ^*_{r50} has run through the selected range by the selected increment, the reference shear that gave the lowest average squared error, while matching the total measured and predicted loads (zero bias), is reported.

Figure 9. Flow Chart of SEDCOMP program algorithm.

Next, *exp* is increased by the defined increment and the calculations are repeated through all the increments of τ^*_{r50}. The result of all these calculations is a list of all the trial exponents (initial value plus all increments) with an associated value of τ^*_{r50} and squared error that matched the total measured and predicted loads. The exponent and τ^*_{r50}

grouping that generated the lowest average squared error are the optimized values for that discharge.

5.3.2 Reference Shear Versus Discharge Relationship

One significant departure of the PKD model from the original Parker-Klingeman bedload function relates to the value of the D_{50} reference shear (τ^*_{r50}) in the hiding factor equation. The original data and analysis from Oak Creek yielded a constant value of 0.0876 relative to the subpavement. Optimization runs using the PKD model for a variety of streams have consistently shown the D_{50} reference shear to systematically vary with discharge (Dawdy et al., 1998). The PKD model allows for this variation by predicting the reference shear from a user input equation that relates reference shear to discharge. This notion will be discussed in more detail in subsequent sections.

5.3.3 Reoptimization with the Average Exponent

Once optimization of the selected samples is complete, optimized pairs of the P-K exponent and D_{50} reference shear result for each discharge. As discussed previously, a relation exists between the reference shear and discharge. This is not the case for the P-K exponent. Instead, the mean of the reported exponents is determined. This initiates a second round of optimization where each sample (or group of samples) is optimized again with the mean exponent. This results in a single set of iterations of the incremented reference shears, which are adjusted to match the total measured and predicted load for the selected mean exponent.

5.4 Rating Curve Prediction

Rating curve prediction for each size class and for total transport rates is done within the FORTRAN program FLOWDUR. This program is a direct application of the

Parker-Klingeman bedload transport model with user input for the previously determined site calibrated P-K exponent and the D_{50} reference shear versus discharge relationship. Output gives annual loads by total and by size class as well as rating curves by total or by size class. A flow chart outlining the FLOWDUR algorithm is shown below. Sample input files and definitions of terms for the FLOWDUR program are listed in Appendix H.

Figure 10. Flow Chart of FLOWDUR program algorithm.

5.5 Site Calibration and Bedload Predictions with Annual Data

Annual Site Calibration. Each bedload measurement was optimized to determine the D_{50} reference shear (relative to the subpavement) and P-K exponent that had the minimum error when predicting both total transport rate and transport rates by size class. Initially, individual years of data were evaluated separately in an attempt to examine annual variation relative to the "true" optimized parameters represented by the entire data set. For each year's data an average P-K exponent was determined and a power function was fit to the reference shear versus discharge data. The results are summarized in the following table.

Table 3. Optimized hiding factor parameters for each year of bedload data at Little Granite Creek.

Year	Avg. Exponent	D_{50} Reference Shear vs. Discharge	R^2
1982	0.979	$\tau_{*r50} = 0.0681\ Q^{0.306}$	0.913
1983	0.975	$\tau_{*r50} = 0.0586\ Q^{0.332}$	0.962
1984	0.979	$\tau_{*r50} = 0.0806\ Q^{0.261}$	0.962
1985	0.973	$\tau_{*r50} = 0.0610\ Q^{0.322}$	0.973
1986	0.981	$\tau_{*r50} = 0.0606\ Q^{0.328}$	0.967
1987	0.972	$\tau_{*r50} = 0.0765\ Q^{0.261}$	0.935
1988	0.973	$\tau_{*r50} = 0.0597\ Q^{0.333}$	0.969
1989	0.976	$\tau_{*r50} = 0.0654\ Q^{0.308}$	0.845
1991	0.960	$\tau_{*r50} = 0.0874\ Q^{0.269}$	0.911
1993	0.969	$\tau_{*r50} = 0.1537\ Q^{0.158}$	0.477
1997	0.972	$\tau_{*r50} = 0.0575\ Q^{0.326}$	0.690
All Years	0.973	$\tau_{*r50} = 0.0680\ Q^{0.302}$	0.925

The annual P-K exponents are expected to be similar throughout the years of data. Multiple comparisons of the annual exponent values were performed using the statistical software package SAS. Methods by Tukey, SNK, and REGW showed no statistical difference between the annual exponents (alpha = 0.05), with the exception of 1991. Note

that all the optimized annual exponents have a magnitude near 1.0, the condition for equal mobility.

As expected, some variability in the reference shear parameters occurs on an annual basis. This variability is consistent with that seen in the individual annual bedload rating curves. Figure 11 graphically illustrates the inverse relation between annual D_{50} reference shear-discharge relations and the actual annual bedload rating curves.

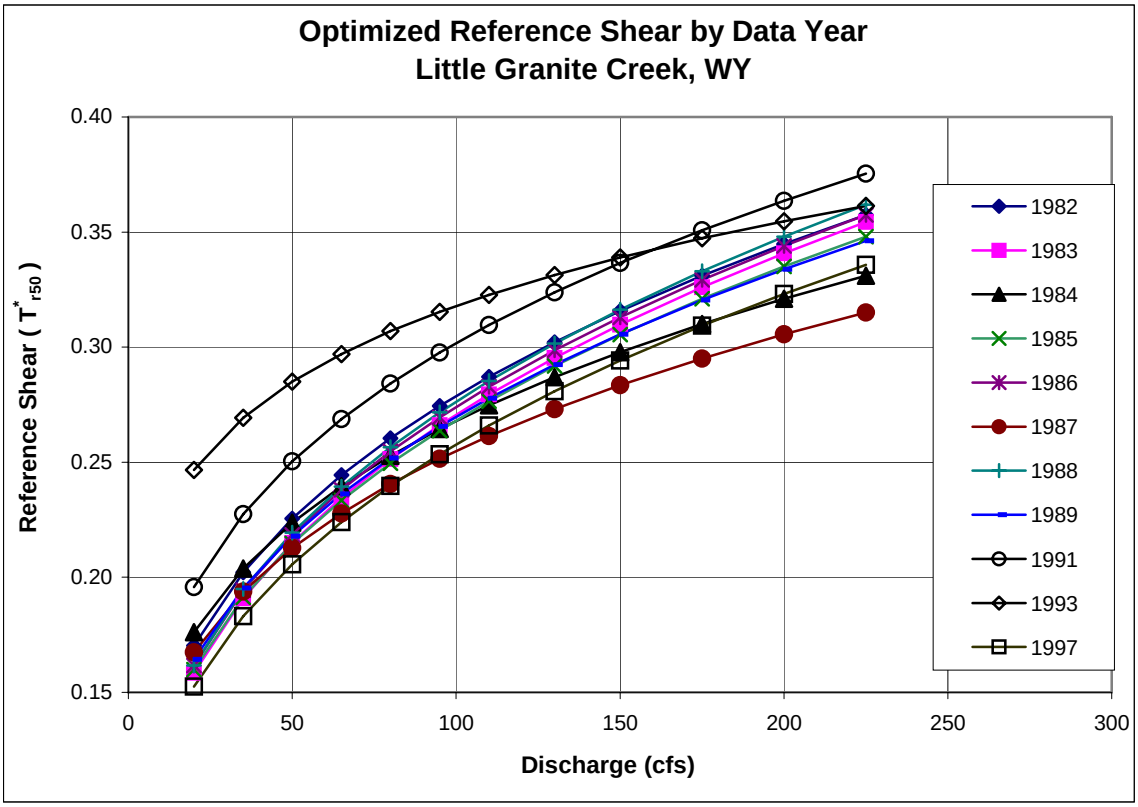

Figure 11. D_{50} reference shear over a selected range of discharges at Little Granite Creek.

For example, data years such as 1991 and 1993 had comparatively low measured transport rates at a given discharge. Figure 11 shows that this results in high reference shear-discharge relationships. Note that a high value of reference shear means that the threshold for initiating motion is high. Similarly, data years 1984, 1987, and 1997 had

comparatively high measured sediment transport rates at given discharge. Consequently they are the three lowest reference shear-discharge relations.

All the relations in Figure 11 have the same basic shape of a power function. Recall that the value of the D_{50} reference shear has typically been considered a constant value resulting from a curve fit (Andrews, 1983; Parker et al., 1982). The basic form of this power function can be mathematically derived by making the approximation that the flow depth is equal to the stage. Solving Equation (13) for this term gives

$$(GH\text{-}e) \approx \text{depth} = (Q/P)^{1/b} \tag{26}$$

Substituting this expression back into the shear relation gives

$$\tau = \gamma\, d\, S = \gamma\, (Q/P)^{1/b}\, S \tag{27}$$

Using this expression in the definition of the Shields stress gives

$$\tau^*_i = \tau / [\gamma\,(s_g\text{-}1) D_i] = \frac{\gamma\,(Q/P)^{1/b}\, S}{\gamma\,(s_g\text{-}1)\, D_i} \tag{28}$$

By making the assumption that the criterion for initiation of motion used by Shields and Parker-Klingeman are approximately equal, the previous expression can be equated to the hiding factor relation as follows

$$\tau^*_i \approx \tau^*_{ri} \rightarrow \frac{\gamma\,(Q_r/P)^{1/b}\, S}{\gamma\,(s_g\text{-}1)\, D_i} = \tau^*_{r50}\,(D_i/D_{50})^{-exp} \tag{29}$$

Where Q_r is the reference discharge associated with the critical condition of motion for some particle size, D_i . Solving the above equation for τ^*_{r50} gives

$$\tau^*_{r50} = \frac{(Q_r/P)^{1/b}\, S}{(s_g\text{-}1)\, D_i}\,(D_i/D_{50})^{exp} \tag{30}$$

For any given calculation with a known sediment size (D_i) and hiding factor exponent (*exp*), most of equation (30) can be expressed as a constant. Rearranging gives

$$\tau^*_{r50} = \frac{(1/P)^{1/b}}{(s_g - 1)\, D_i} \frac{S\,(D_i/D_{50})}{exp}\ (Q_r)^{1/b} \quad (31)$$

$$\tau^*_{r50} = \text{constant}\ (Q_r)^{1/b} \quad (32)$$

Recall from Equation (14) that the stage-discharge relationship for Little Granite yielded b = 2.36. Therefore, the exponent in the D_{50} reference shear versus discharge relationship is 1/b = 0.42. This is a reasonable approximation of the annual values listed in Table 3 given that the annual values were optimized from incremental depth measurements across the channel while the value from Equation (31) was approximated from a single stage reading. Equation (31) is plotted with the individually optimized D_{50} reference shear values in Figure 14 for $D_i = D_{50}$.

Annual Bedload Predictions. Bedload rating curves are predicted using the Parker-Klingeman transport model with known values in the hiding factor relationship. If the hiding factor parameters are accurately optimized, the Parker-Klingeman model will predict a rating curve that passes directly through the collection of measured bedload rates (either total or by size class). An example of total transport rates is shown in Figure 12 for the 1986 data. Note that the least squares regression line and the predicted PKD rating curve are nearly the same. This is typically the case for each year of data.

The advantage of the PKD prediction over a simple regression approach (with limited data values) is that the model provides a coupled prediction between total load and load by size class. This coupling occurs through the hiding factor in Equation (4). The rating curves by size class for the 1986 data graphically illustrate this point, particularly for the larger particle sizes. The largest particles have both a low probability of being caught and might even be too large to fit in a Helley-Smith sampler. With these two limitations, the prospect of using measured data to predict the rating curve for

particles greater than 32-mm is poor. The modified Parker-Klingeman model (with local optimization) is able to predict movement of these particles based on their availability in the bed and their reference shear calculated as a function of the neighboring particles. Measured data and predicted bedload rating curves with the PKD model are shown by size class in Figure 13.

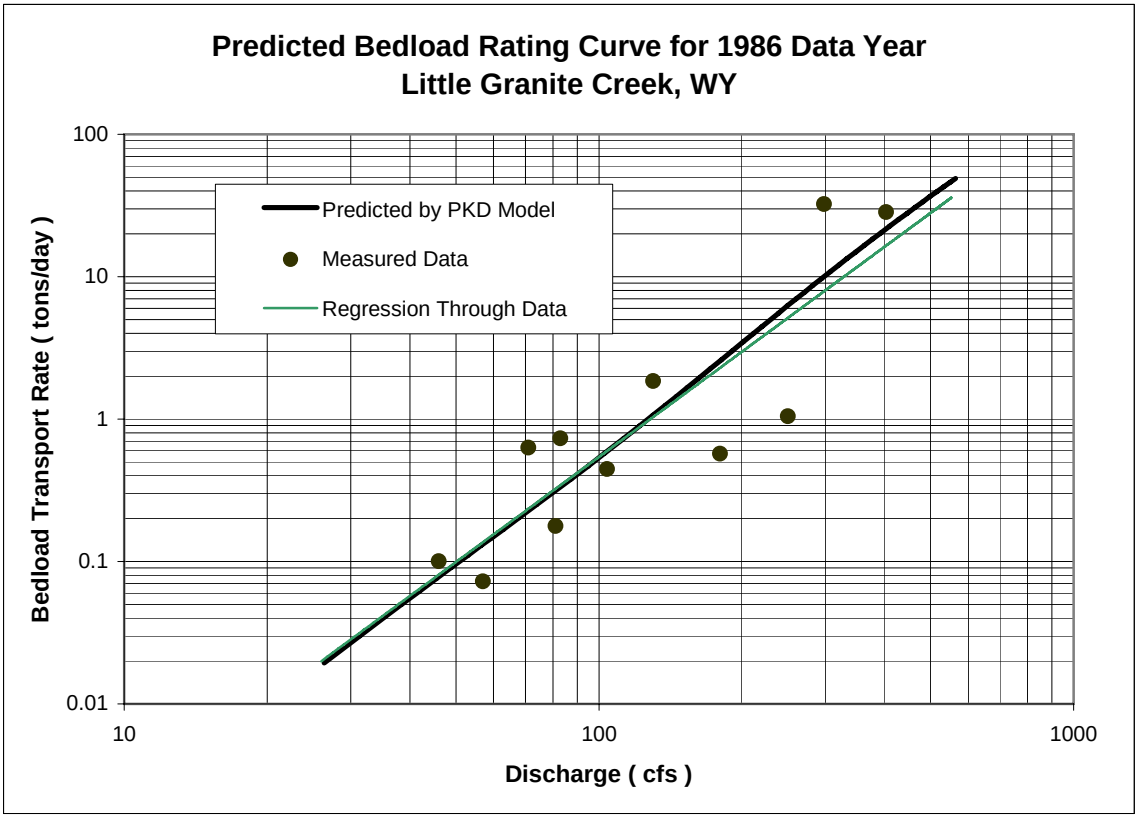

Figure 12. Predicted total bedload rating curve for data year 1986 at Little Granite Creek

5.6 Site Calibration and Bedload Prediction with the Entire Data Set

Site Calibration for All Years. All the optimized D_{50} reference shear and exponent values for each discharge are now collectively analyzed, independent of the year of collection. The plot of the optimized reference shear versus discharge shown in Figure 14 again takes the form of a power function. The average value of all the

optimized P-K exponents is 0.973. The distribution of the values of this exponent is approximately normal with a standard deviation of 0.013.

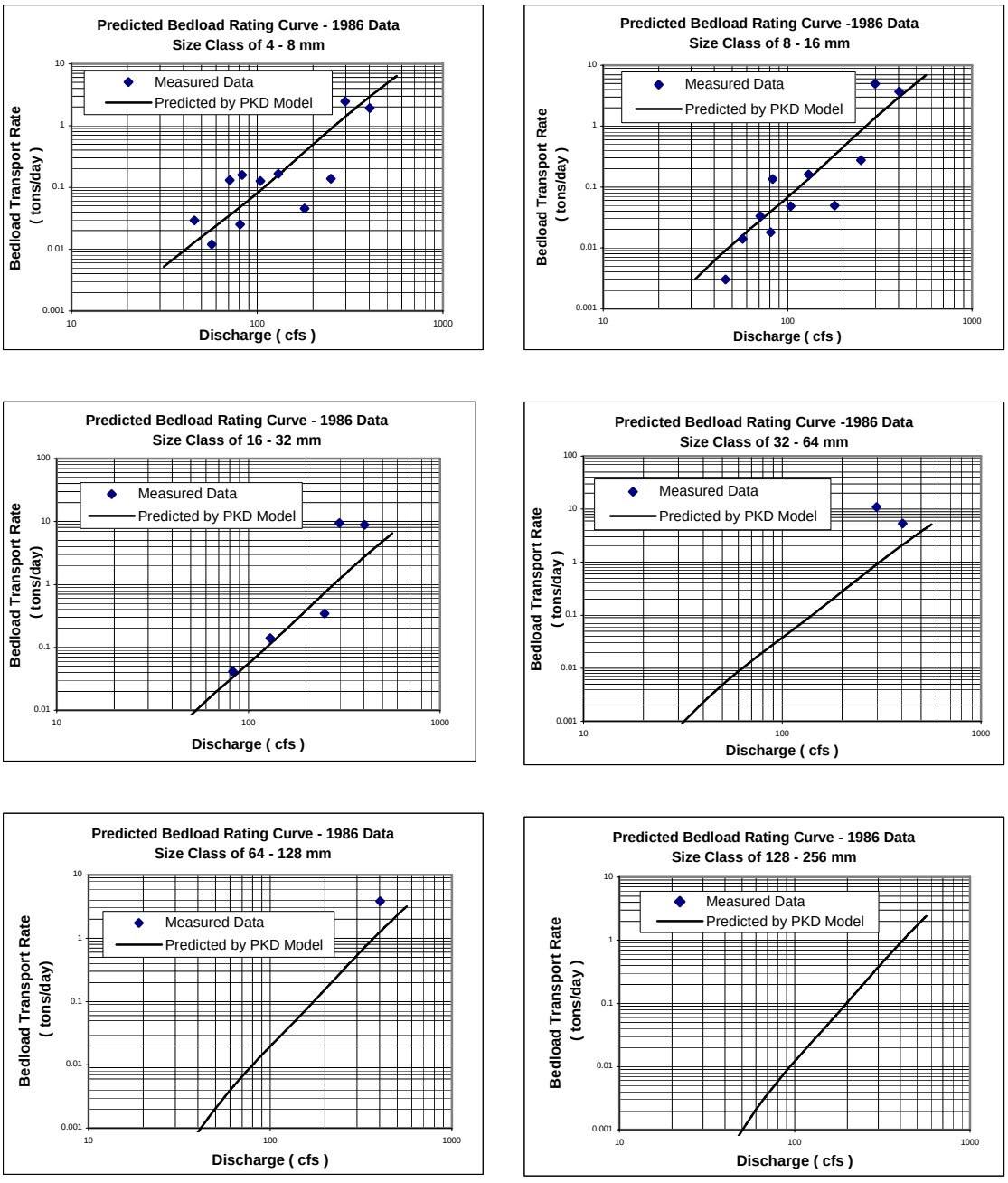

Figure 13. Predicted bedload rating curves for selected size classes for data year 1986 at Little Granite Creek.

For comparison, default hiding factor parameters from the original Parker-Klingeman model using the Oak Creek, Oregon data are shown below. Predicted bedload transport rates using these default values were discussed in Chapter IV.

Table 4. Hiding factor parameters for Little Granite Creek, WY and Oak Creek, OR.

Predictive Equation	Data Source	P-K Exponent	τ^*_{r50} vs. Q Relation
Site Calibrated PKD Model (Bakke et al., 1999)	Little Granite Creek, WY	0.973	$\tau^*_{r50} = 0.0680\ Q^{0.302}$
Parker and Klingeman (1982)	Oak Creek, OR	0.982	$\tau^*_{r50} = 0.0876$ = Constant

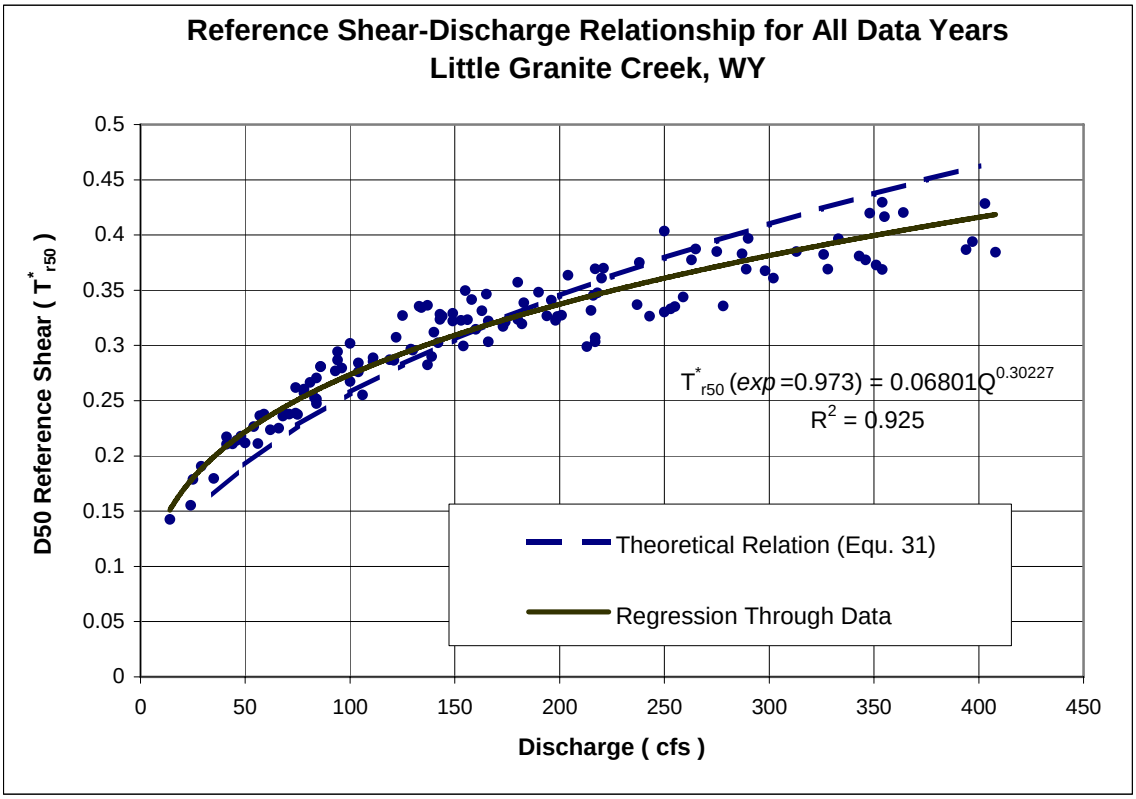

Figure 14. D_{50} reference shear versus discharge for all data points at Little Granite Creek.

Bedload Predictions for All Years. To evaluate the effectiveness of the model's predictions relative to the measured data set, Figure 15 shows a plot of measured and calculated transport rates. The measured-calculated pairs are approximately equally

distributed above and below the “equal fit” line. This would suggest that the predicted rating curve should look very similar to a “best fit” line through the data.

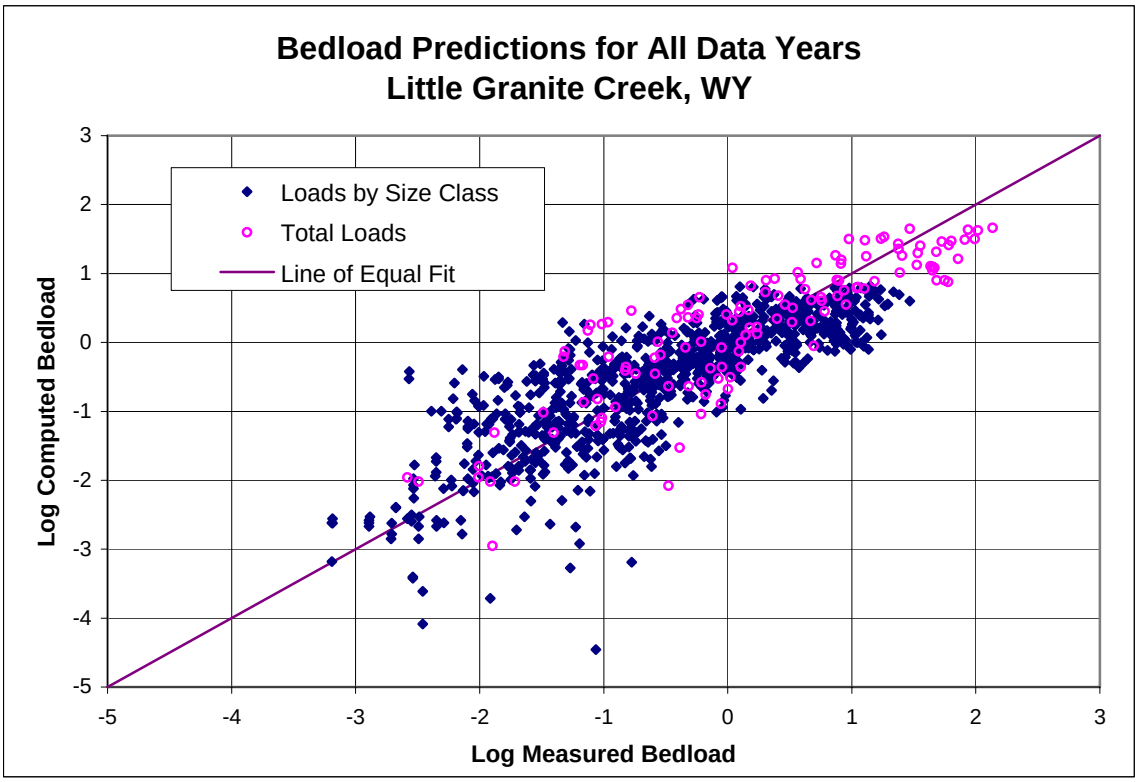

Figure 15. Measured and calculated transport rates for entire data set at Little Granite

The predicted bedload rating curves using hiding factor parameters from optimizing all the data points are shown in Figures 16 and 17. Predicted rating curves using the conventional models are also shown again for comparison. Note that the variability in transport rates by size class is relatively small. This condition of near-equal mobility is consistent with the P-K exponent value being very close to 1.0.

The locally calibrated hiding factor parameters effectively adjusted the predicted transport rates to match those measured. This is of particular interest since the majority of the measured bedload is washload. This significant adjustment in predicted transport rates

can also occur within the Meyer-Peter and Müller equation by substituting the previously optimized hiding factor parameters for τ^*_c. Recall that τ^*_c (or τ^*_r) is calculated as

$$\tau^*_r = \tau^*_{r50} (D_i / D_{50})^{-exp} \quad (4)$$

Where $exp = 0.973$ for Little Granite Creek and the reference Shields stress relative to the D_{50} was previously determined to be

$$\tau^*_{r50} = 0.0680 Q^{0.3023} \quad (33)$$

The rating curves determined in this manner are also shown in Figure 16. Note that the Meyer-Peter and Müller equation with the default value of $\tau^*_c = 0.047$ causes an over prediction of orders of magnitude. The Meyer-Peter and Müller predictions (for both pavement and subpavement) using the site-specific hiding factor more closely approximate the measured data.

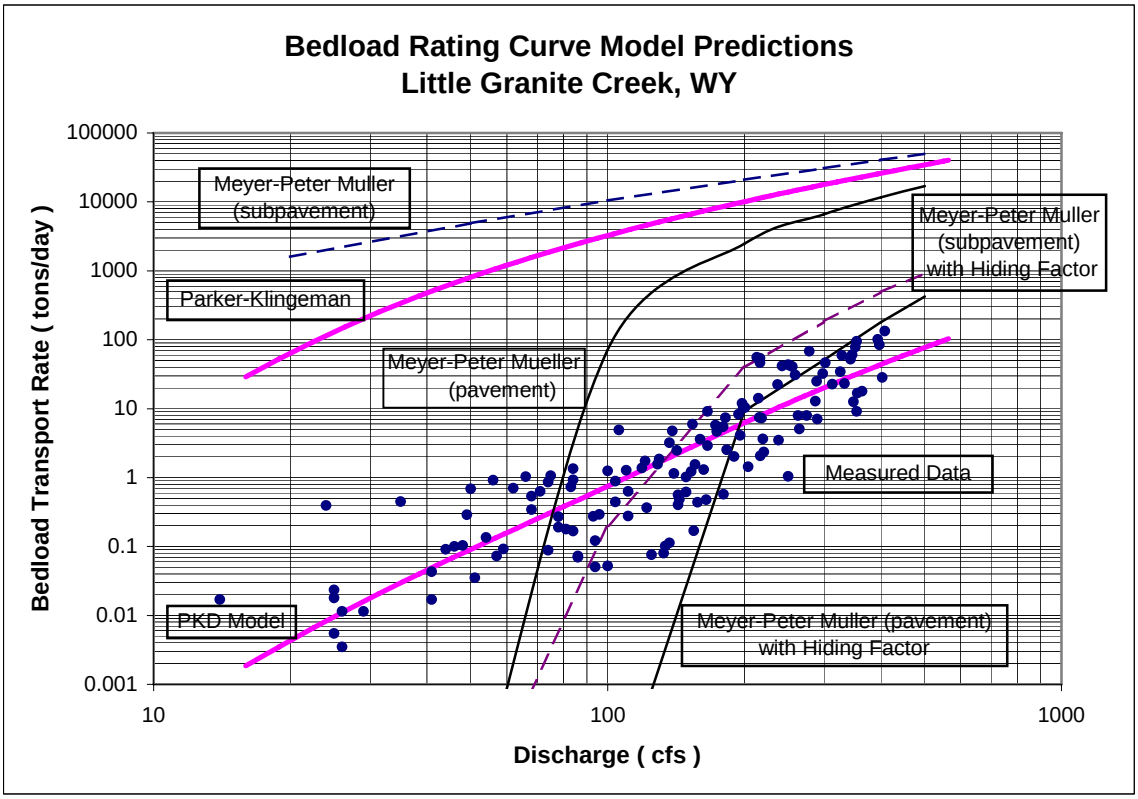

Figure 16. Total bedload rating curve for all data years at Little Granite Creek

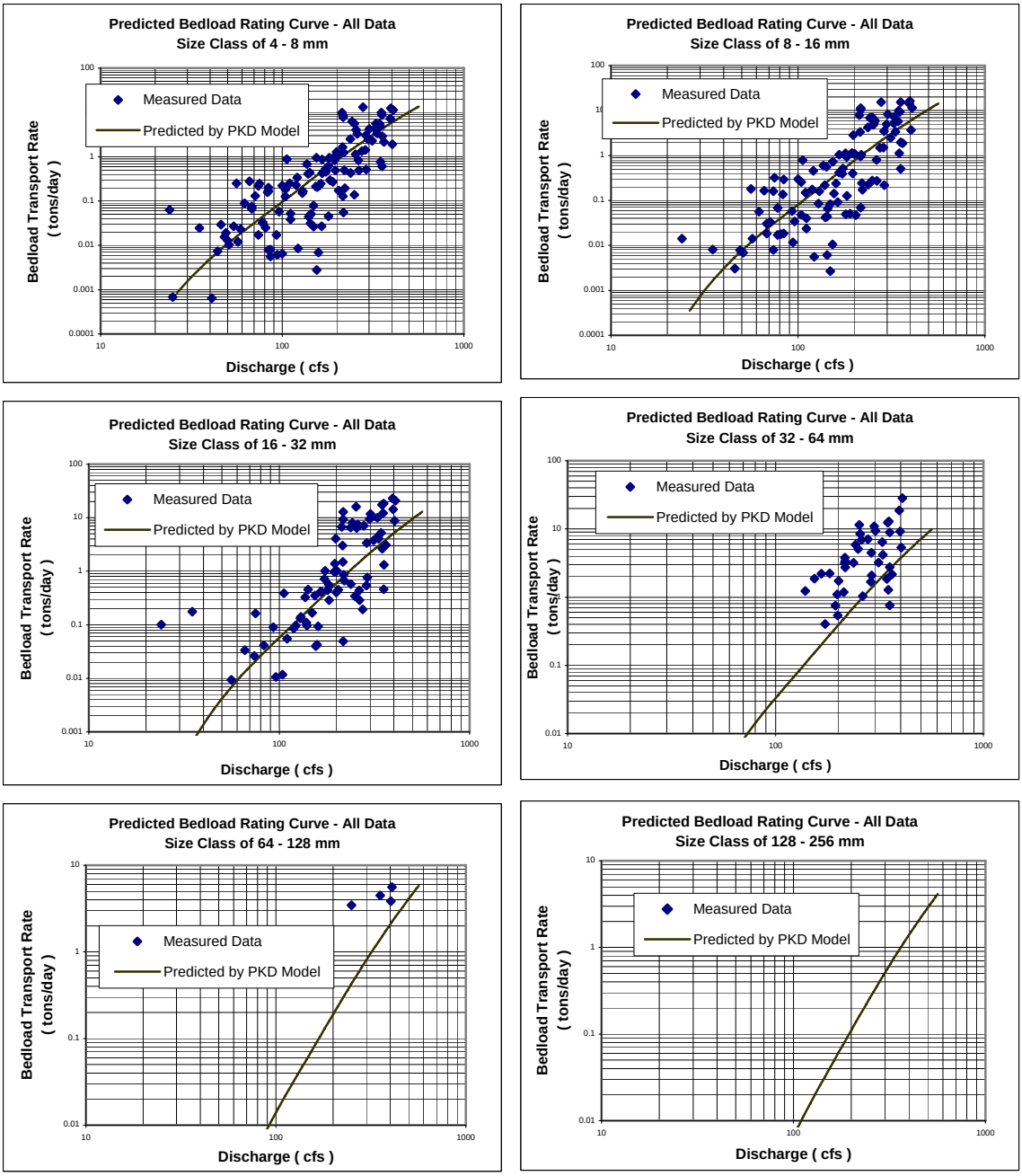

Figure 17. Predicted bedload rating curves for selected size classes for all years of data at Little Granite Creek.

Chapter 6: Evaluation of Model Sensitivity to Bedload Sample Inputs

6.1 Background and Assumptions

The site calibrated PKD model requires a number of input parameters for parameter optimization and general hydraulic computations. The input parameter that allows the most user judgment is the number and range of actual measured bedload samples used to calibrate the model. *The intent of this analysis is to examine the variability in the model predictability as the input sample size changes*. This will be accomplished by developing a bootstrapping algorithm to sample with replacement from the original bedload data set and develop subsets of data for model calibration. Each bootstrap sample set and associated model runs will yield a distribution of the pertinent hiding factor parameters, which can then be compared to the "true" values from the entire data set.

The accuracy of the model prediction will be determined by how well the sampled parameters match the "true" values of the P-K exponent, D_{50} reference shear, and total annual load. The "true" P-K exponent for the entire data set at Little Granite was 0.9727. The "true" value of the D_{50} reference shear was determined by recreating Figure 14, except that the reference shears were not reoptimized with a common P-K exponent. The resulting expression is of the form

$$\tau^*_{r50} = \alpha Q^{\beta} \qquad (34)$$

where $\alpha = 0.0688$ and $\beta = 0.3011$. The "true" value of total annual bedload is that determined from the Parker-Klingeman bedload model using the "true" values for the P-K exponent and D_{50} reference shear-discharge relation.

Bedload subsample sizes of three, six, ten, fifteen, twenty, and thirty were selected. A subsample size of three was selected as the minimum, primarily to show the variability that can occur from such a small sample size. Thirty was selected as the maximum subsample size since that value is often quoted as a minimum necessary to construct purely statistical bedload rating curves.

A fundamental assumption of bootstrapping is that the data are independent. However, the parent data sets of both stream flow and sediment discharge are correlated on a time series, a common test of data independence. The effects of violating this assumption are unknown.

A second assumption is that the set of discrete measurements at Little Granite Creek are assumed to adequately represent the continuous variables of discharge and bedload transport rate.

6.1.1 Parameters of Interest

Since one of the ultimate goals of using the SEDCOMP model is to predict a bedload rating curve, it would follow that the accuracy of the predicted rating curve should be used to evaluate the effects of sample size. However, the process involved in predicting the rating curve is somewhat iterative and involves more than one software package, making a comparison to a "true" value difficult. A surrogate for the bedload rating curve was required. The accuracy of the Parker-Klingeman bedload function has been shown to depend on accurate selection of the P-K exponent and D_{50} reference shear versus discharge relationship for the site (see Chapter V). Consequently, the sampled

values of the P-K exponent, D_{50} reference shear relationship (α and β), and total annual load will be compared to the "true" values for the entire data set, instead of the predicted bedload rating curve.

A necessary shortcut in this process is the elimination of the final optimization of D_{50} reference shear values to match the average P-K exponent. This iteration was not possible within a Minitab macro. The data set for Little Granite Creek suggests that the error involved by omitting this second step is slight. For the eleven years of data collected and optimized separately, the final regression lines of D_{50} reference shear and discharge for the optimized points and the reoptimized (common P-K exponent) points varied only slightly.

6.1.2 Bootstrapping

Bootstrapping is a sampling method with replacement used to determine the accuracy of an estimated parameter based on a sample, rather than an assumed distribution (Efron and Tibshirani, 1993). A bootstrap begins with a random sample of size n, which is drawn from an unknown probability distribution. The parent data set (size = N) is sampled with replacement B times where each observation has a 1/N chance of being selected. The statistic of interest is then calculated for each of the B subsamples.

As applied to this specific analysis, B random samples are taken for each subsample size of n = 3, 6, 10, 15, 20 and 30. Each individual observation has a 1/133 chance of being selected for Little Creek. Once the subsample is obtained, the parameters of interest (α, β, *exp*, total annual load) are calculated.

To determine the number of bootstrap samples B, the variance of the subsample estimates was visually examined for each of the subsample sizes. The number of bootstrap samples was considered adequate when the variance of the subsample estimates

became approximately constant with increasing bootstrap iterations (Rudy King, personal communication, 2000). The worst-case was for a subsample of three, where the variance versus bootstrap iteration relation did not become constant until about 900 iterations. The number of iterations required for the larger subsample sizes to reach a steady variance was considerably smaller. The number of random samples, B, was conservatively set at 1000 for this analysis.

The statistical software package Minitab was used to do the random sampling, curve fits, and variance analysis. A macro was written within Minitab to randomly select samples of the previously optimized bedload samples, compute the average P-K exponent, and curve fit a power function to the D_{50} reference shear versus discharge data. The sampled values of α, β, and P-K exponent were used to calculate the total annual load using the Parker-Klingeman model. The resulting values of α, β, P-K exponent, and total annual load define a particular subsample.

With the exception of the subsample size of three, there were enough sampled points to reasonably curve fit the reference shear-discharge relation. The subsample size of three was small enough that the variability of D_{50} reference shears at similar discharges had a significant weighting effect on the regression line, which caused wildly inaccurate predictions. To counter this, an extra line of code was added to the sampling macro (only for n=3) that required each measurement to be at least 20 cubic feet per second (cfs) away from the other measurements. Even with this stipulation the predictions for a subsample size of three were highly variable.

6.2 Random Sampling Results

The boxplots (Figures 18-21) show the distribution of the resulting estimates of the parameters of interest for the 1000 bootstrap iterations. For each individual box, the top and bottom represent the 25^{th} and 75^{th} percentiles. The length of the box is the inter-quartile range (IQR), which contains fifty percent of the data. The whiskers on the ends of the box extend out 1.5 times the IQR, if data extend that far. The range is considered the length of the box and whiskers combined. Any data point falling outside the range is considered an outlier and is denoted by a star. The horizontal line inside the box represents the median of the subsamples. To facilitate comparison of the boxplots across subsample size, the lengths of the IQR and range are used. A small inter-quartile range is desired, which suggests that many of the data are tightly grouped around the median. By similar reasoning it is desirable to have a small range as well.

Note that two sets of boxplots are shown for the parameters of the power function coefficient α and the total annual load. The first boxplots show the relevant statistics for all subsample sizes. The second boxplots exclude the subsample sizes of three and six because the extreme values predicted with those subsample sizes do not allow the variability among the larger subsample sizes to be recognized.

It is apparent that relative differences from the "truth" decrease with sample size. The improvement is not linear, but rather has somewhat diminishing returns with increasing sample sizes. In other words, doubling the subsample size does not halve the relative difference of the parameter of concern. This is numerically quantified in the following table using the interquartile range, median, and the mean as the basis of comparison as sample size changes.

Table 5. Variability of bootstrap parameters of interest with subsample size.

		n = 3	n = 6	n = 10	n = 15	n = 20	n = 30	"Truth"
P-K Exp	IQR	0.0093	0.0067	0.0055	0.0046	0.0038	0.0032	
	Median	0.9737	0.9727	0.9727	0.9729	0.9728	0.9730	
	Mean	0.9732	0.9727	0.9727	0.9728	0.9729	0.9728	0.9727
α coeff.	IQR	0.0400	0.0207	0.0157	.01272	0.0108	0.0082	
	Median	0.0716	0.0703	0.0702	0.0692	0.0695	0.0694	
	Mean	0.1030	0.0767	0.0733	0.0711	0.0707	0.0701	0.0688
β exponent	IQR	0.108	0.060	0.046	0.036	0.030	0.024	
	Median	0.290	0.296	0.296	0.299	0.299	0.300	
	Mean	0.274	0.291	0.293	0.297	0.297	0.298	0.301
Total Load	IQR	130.0	56.2	35.6	28.9	23.0	19.9	
	Median	90.0	58.0	51.7	48.2	47.0	45.7	
	Mean	521.0	130.2	58.2	53.2	50.0	47.8	48.3

In all instances, substantial decreases in both the range and IQR occur from a subsample size of three to a subsample size of six. A similar but somewhat smaller improvement occurs between subsamples of six and ten. The improvement from ten to fifteen, fifteen to twenty, and twenty to thirty are consistent but more modest. For all the parameters of concern, the average decrease in the IQR as the sample size increased from three to six was 45 percent. The decreases in the IQR as the sample size changed from six to ten, ten to fifteen, fifteen to twenty, and twenty to thirty were 26%, 19%, 17% and 19%, respectively. This depiction of the diminishing returns with sample size might suggest a minimum sample size of ten or fifteen as a starting point. At a subsample size of 10-15, both the mean and median are a reasonable approximation of the "true" values of interest and much of the reduction in IQR has been attained.

The distributions of the P-K exponent are the only ones with no skew and very few outliers. They represent the closest approximation of a normal distribution. The power function coefficient α is right skewed but loses most of its extreme predicted values as sample size increases above fifteen. The power function exponent β is slightly right skewed with little change in the spread above a sample size of fifteen. The total load

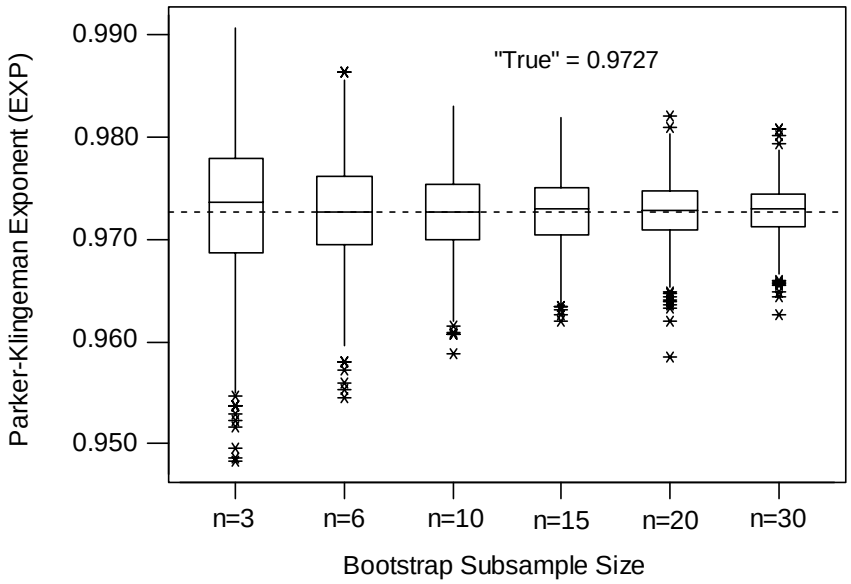

Figure 18. Boxplots of 1000 random sample estimates of P-K exponent for Little Granite Creek.

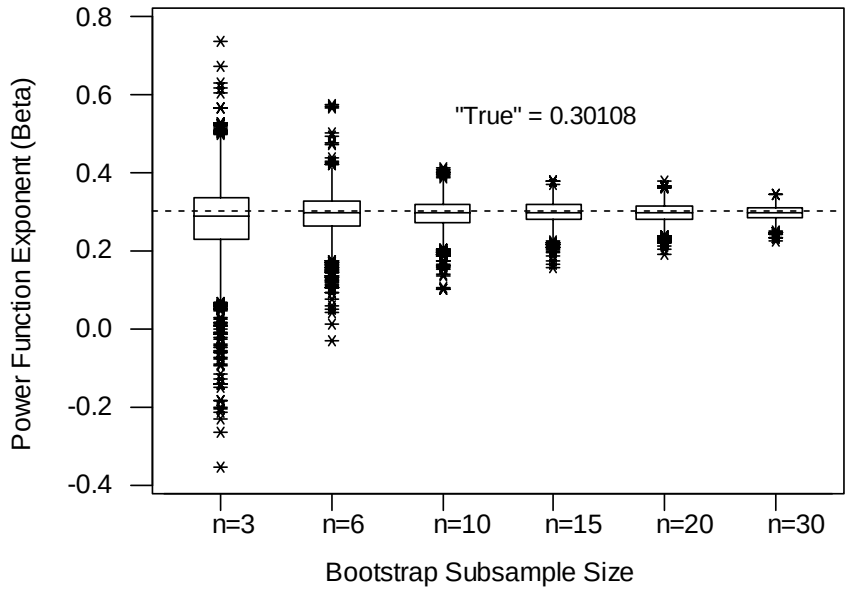

Figure 19. Boxplots of 1000 random sample estimates of power function exponent β.

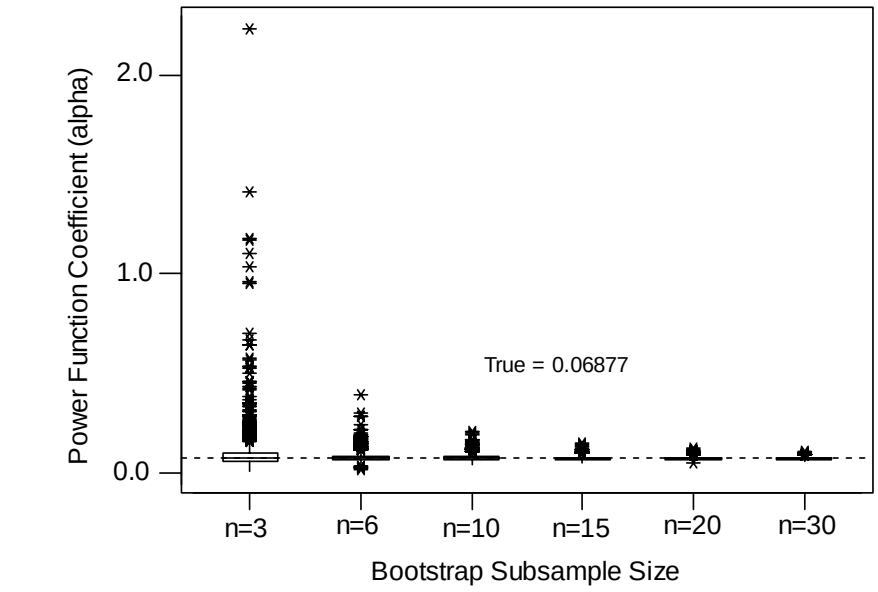

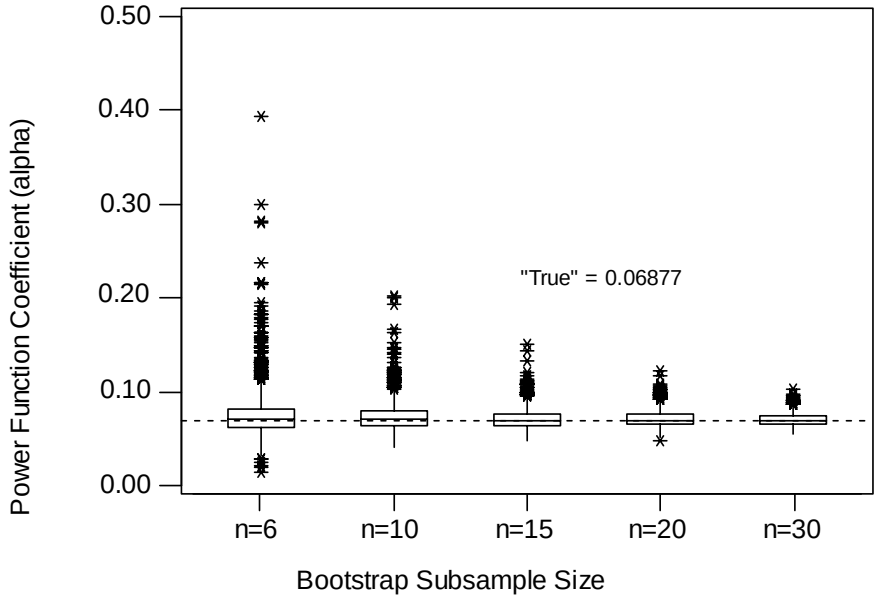

Figure 20. Boxplots of 1000 random sample estimates of power function coefficient α.

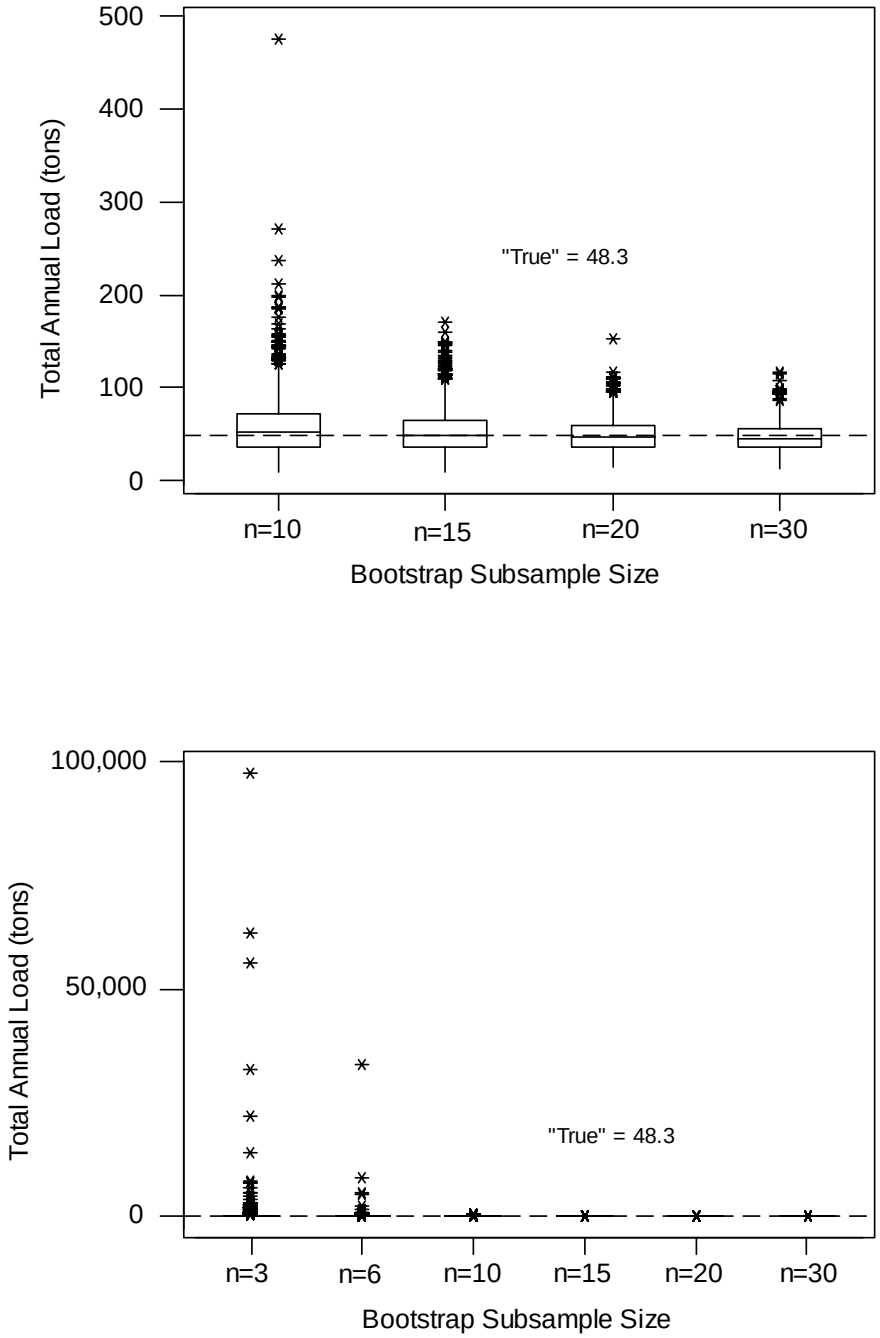

Figure 21. Boxplots of 1000 values of computed total annual load for sampled parameters.

distributions are strongly right skewed since it is bounded by zero load. The possibility of very extreme values exists up through a sample size of ten and begins to decrease above sample size of fifteen.

While the boxplots and Table 5 all give some guidance on selection of an appropriate sample size, a more quantitative approach would still be of use. Since the parameters of interest do not have normal distributions for all sample sizes, a non-parametric approach is appropriate. The notion of selecting the sample size based on acceptable error is evaluated for the parameters of interest.

To accomplish this, cumulative distribution functions (CDF) for the relative differences of the parameters of interest are generated from the bootstrap data sets. These allow a user, knowing the maximum acceptable value of the relative error, to determine what percentage of subsamples might meet this requirement. This approach relies on a relative frequency concept of probability.

The cumulative distribution functions for each parameter of interest are shown on Figures 22-25. For clarity, the actual stepped shape of the functions was approximated as a continuous smoothed curve through the center of each x-axis bin. Using Figure 22 as an example, suppose you wanted to find the sample size that would give a maximum one percent relative error for the P-K exponent at least 80 percent of the time. The user would enter into Figure 22 on the x-axis at one percent then cross the sample size plots until the intersection is above 80% on the y-axis. This would be the sample size that produced a relative error of one percent or less, 80 percent of the time in repeated sampling.

A similar exercise can be done with the figures for α, β and total annual load. This, at the very least, provides some loose confidence measures to the sampled parameters. A confounding situation arises in that we do not know the effect on the

bedload rating curve of the error in the P-K exponent, α or β. This is especially true since the relative errors given are absolute values and do not show whether the error is an over or under prediction. Consequently, an exhaustive sensitivity analysis of the hiding factor parameters on the predicted bedload rating curve would be required.

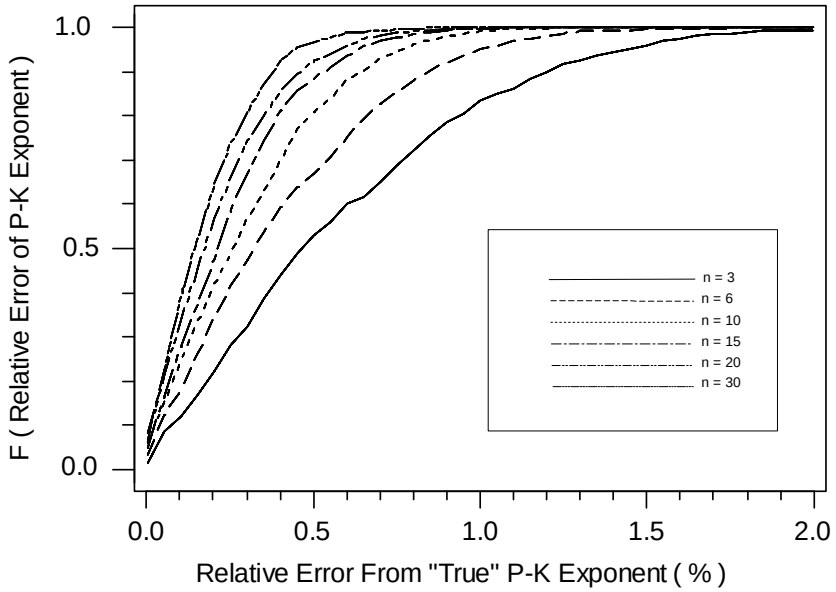

Figure 22. Cumulative distribution of relative error between "true" and sample estimates of P-K exponent.

In order to visualize the effects of the spectrum of variation in the hiding factor parameters on the predicted bedload rating curve, the total annual load is used. Figure 25 shows the cumulative distribution function for the total annual bedload in tons. Note that the shapes of these distributions are considerably flatter with increasing error than the other plots. This suggests that, for a given subsample size and relative error, there is a lower probability of that event occurring. This is expected since Figure 25 incorporates all the error from the P-K exponent, α, and β. Also, the error is compounded by multiple

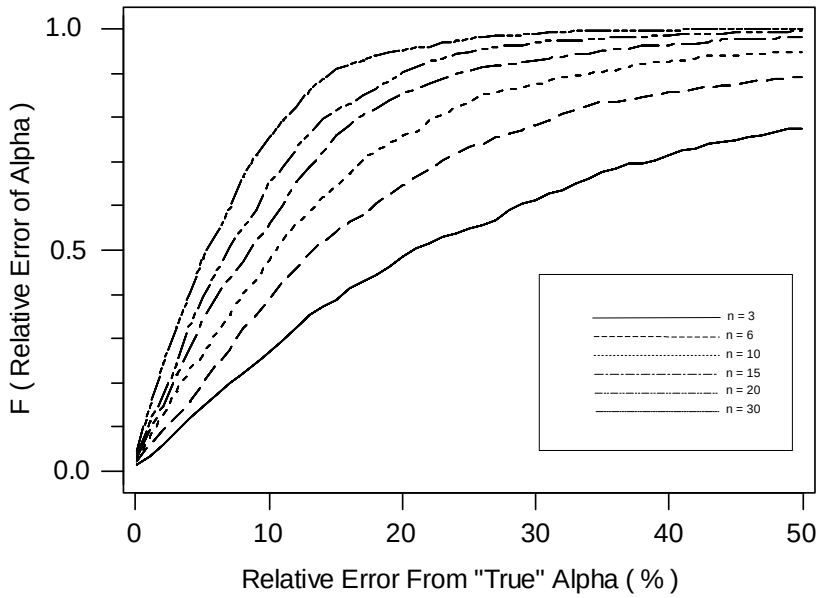

Figure 23. Cumulative distribution of relative error between "true" and sample estimates of α.

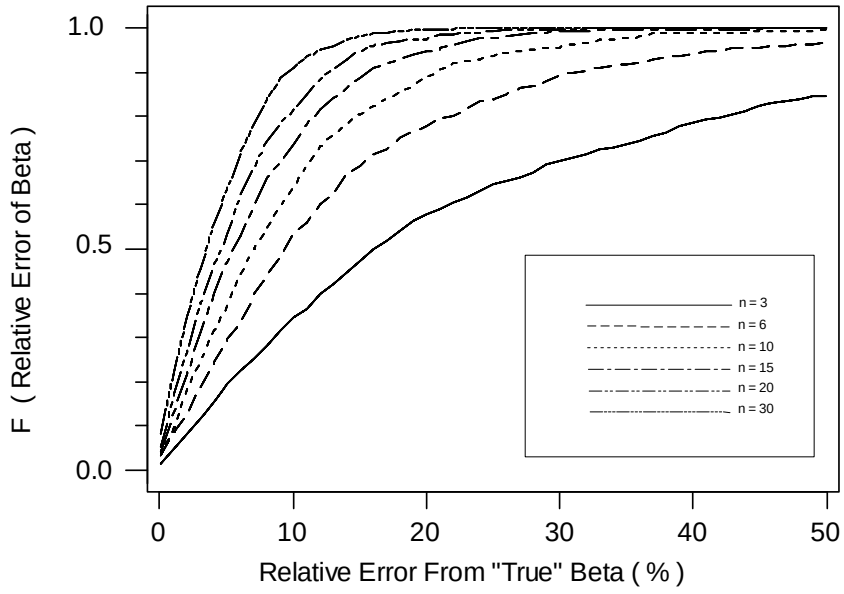

Figure 24. Cumulative distribution of relative error between "true" and sample estimates of β.

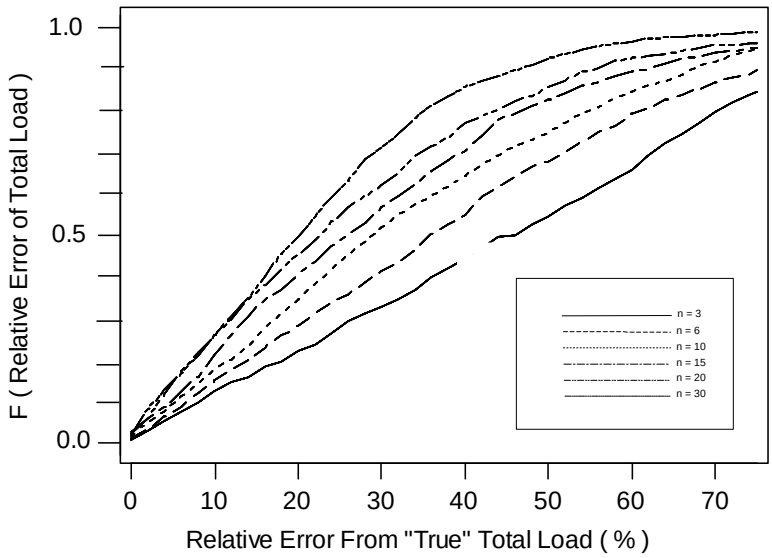

Figure 25. Cumulative distribution of relative error between "true" and calculated total annual load.

applications of the Parker-Klingeman bedload transport model at all the discharges in the flow duration curve.

Boxplots and cumulative distribution functions provide a means of selecting an input sample size for bedload measurements in the PKD model. The boxplots provide some measure of the mean, median and variability of the predicted values. The cumulative distribution functions allow the user to select the sample size based on an acceptable relative error from the "true" values of the total data set.

Chapter 7: Summary and Conclusions

1. The hiding factor relationship (Equation 4) includes two parameters, the P-K exponent and reference shear associated with the D_{50}, that vary by stream. Incrementally adjusting these two parameters, until the measured and predicted loads are equal, allows for site-calibration of the Parker-Klingeman bedload transport model. For Little Granite Creek, the P-K exponent averaged 0.973 for all data years, compared to a value of 1.0 for equal mobility of all sediment sizes. The value of the D_{50} reference shear (τ^*_{r50}), generally considered a constant, was shown to increase with discharge as a power function.

2. The majority of the measured bedload in Little Granite Creek appears to be supply limited. The most conservative estimate, based on the D_{10} particle size of the pavement, suggests that bedload finer than 11-mm is washload. These grain sizes account for most of the measured load at low and intermediate discharges. This is supported by the observation that years preceded by high flows typically had higher than average sediment transport rates at a given discharge. Years preceded by low flows typically had lower than average bedload transport rates. Antecedent conditions of the annual maximum mean daily flow appear to provide a simple means of checking that both high and low bedload transport rates are being sampled for a bedload rating curve.

3. Traditional predictive equations of Meyer-Peter and Müller, Einstein-Brown, and Parker-Klingeman all grossly over predict the measured sediment transport rates for Little Granite Creek. These models predict transport capacity of bed-material load and assume an unlimited supply of material for transport. The coarse pavement layer at Little

Granite Creek effectively limits the availability of finer grained particles until that layer is disturbed. Replacing the critical (reference) Shields stress term with the expression for the site-calibrated hiding factor in both the Meyer-Peter and Müller and Parker-Klingeman models cause these equations to predict transport rates similar to those measured. This is noteworthy since most of the measured load is washload.

4. Bootstrapping techniques were used as a mechanism to examine the variability of the PKD model predictions as the bedload subsample size changed. As bedload subsample size increases, the accuracy of the prediction of the hiding factor parameters increases. For Little Granite Creek, the largest reduction in the prediction variability is attained by using a minimum of ten to fifteen bedload samples collected over a range of discharges and antecedent conditions. A cumulative frequency distribution of total annual load provides a method of refining that subsample size based on an acceptable error from the "true" value based on the entire data set.

Bibliography

Andrews, E.D. 1983. Entrainment of gravel from naturally sorted riverbed material. GEOL. SOC. AMER. BULLETIN, 94: 1225-1231.

Andrews, E.D. and Erman, D.C. 1986. Persistence in the size distribution of surficial bed material during an extreme snowmelt flood. WATER RESOURCES RESEARCH, 22(2):191-197.

Andrews, E.D. and Parker, G. 1987. Formation of a coarse surface layer as the response to gravel mobility. In: *Sediment Transport in Gravel Bed Rivers*. C.R. Thorne, J.C. Bathurst and R.D. Hey (eds.). John Wiley and Sons, Chichester. pp. 269-325.

Andrews, E.D. and Nankervis, J.M. 1995. Effective Discharge and the design of channel maintenance flows for gravel-bed rivers. NATURAL AND ANTHROPOGENIC INFLUENCES IN FLUVIAL GEOMORPHOLOGY. Geophysical monograph 89.

Bakke, P.D., Basdekas, P.O., Dawdy, D.R., and Klingeman, P.C. 1999. Calibrated Parker-Klingeman model for gravel transport. JOURNAL OF HYDRAULIC ENGINEERING, ASCE. Vol. 25. No. 6. pp. 657-660.

Bathurst, J.C. 1987. Critical conditions for bed material movement in steep, boulder-bed streams. In: *Erosion and Sedimentation in the Pacific Rim*. IAHS Publication no. 165, Institute of Hydrology, Wallingford. pp. 309-318.

Brown, C.B. 1950. Sediment transportation. In: *Engineering Hydraulics*. H. Rouse, ed. John Wiley and Sons, New York, NY. pp. 769-857.

Bunte, K. and Abt, S. 1999. Draft Sampling surface and subsurface particle-size distributions in gravel-bed streams for analyses in sediment transport, hydraulics, and stream bed monitoring. Version 6. Report prepared for the Stream Systems Technology Center, Rocky Mountain Forest and Range Experiment Station, Fort Collins, CO. 253 pp.

Burkam, D.E. and Dawdy, D. R. 1976. Resistance equations for alluvial-channel flow. JOURNAL OF THE HYDRAULICS DIVISION, ASCE. Vol. 102. No. HY10. pp 1479-1489.

Carson, M.A., and Griffiths, G.A. 1985. Tractive stress and the onset of bed particle movement in gravel stream channels: different equations for different purposes. JOURNAL OF HYDROLOGY, 79: 375-388.

Chang, H.H. 1998. *Fluvial Processes in River Engineering*. Krieger Publishing Company, Malabar, FL. 432 pp.

Chien, N. 1956. The present status of research on sediment transport. TRANS. ASCE. 121:833-868.

Church, M. 1985. Bed load in gravel-bed rivers: Observed phenomena and implications for computation. Canadian Society for Civil Engineering Annual Conference. p 17-37.

Church, M., McLean, D.G., and Walcott, J.F. 1987. River bed gravels: sampling and analysis. In: *Sediment Transport in Gravel Bed Rivers*. C.R. Thorne, J.C. Bathurst and R.D. Hey (eds.). John Wiley and Sons, Chichester. pp. 43-79.

Dawdy, D.R., Wang, W.C., and Basdekas, P.O. 1998. Calibration of the Parker-Klingeman model with variable shear. In: *River Sedimentation: Theory and Applications.* Proceedings of the seventh international symposium on river sedimentation. A.W. Jayawardena, J.H. Lee, and Z. Y. Wang (eds.). Ashgate Publishing, Rotterdam. 1088 pp.

Efron, B. and Tibshirani, R.J. 1993. *An Introduction to the Bootstrap*. Chapman and Hall, New York, NY. 436 pp.

Egiazaroff, I.V. 1965. Calculation of nonuniform sediment concentrations. JOURNAL OF THE HYDRAULICS DIVISION, ASCE. Vol. 91, No. HY4, pp. 225-247.

Einstein, H.A. 1942. Formulas for the transportation of bed load. TRANS. ASCE. 107: 561-573.

Einstein, H.A. 1950. The bed-load function for sediment transport in open channel flows. TECHNICAL BULLETIN No. 1026, U.S. Department of Agriculture, Soil Conservation Service.

Emmett, W.W. 1998. United States expert witness report of Dr. William W. Emmett concerning Organic Act claims. Snake River basin adjudication. Boise, ID. 92 pp.

Emmett, W.W. 1999. Quantification of channel-maintenance flows for gravel-bed rivers. In: *Wildland Hydrology*. D.S. Olson and J.P. Potyondy (eds.). TPS-99-3. American Water Resources Association. Herndon, VA. pp. 77-84.

Fenton, J.D., and Abbott, J.E. 1977. Initial movement of grains on a stream bed: the effect of relative protrusion. Proc. Royal Society of London, Series A, 352: 523-537.

Gilbert, R.O. 1987. *Statistical Methods for Environmental Pollution Monitoring*. John Wiley & Sons, New York, NY. 320 pp.

Hollinghead, A.B. 1971. Sediment transport measurements in a gravel-bed river. JOURNAL OF THE HYDRAULICS DIVISION, ASCE. Vol. 97, No. HY11, Proc. Paper 8521, pp. 1817-1834.

Julien, P.Y. 1995. *Erosion and Sedimentation*. Cambridge University Press, New York, NY. 280 pp.

King, Rudy. Station statistician for Rocky Mountain Research Station. Fort Collins, CO. Personal communication during July 2000.

Komar, P.D. 1987a. Selective gravel entrainment and the empirical evaluation of flow competence. SEDIMENTOLOGY, 34:1165-1176.

Komar, P.D. 1987b. Selective grain entrainment by a current from a bed of mixed sizes: a reanalysis. JOURNAL OF SEDIMENTARY PETROLOGY. 57:203-211.

Leopold, L.B. 1992. Sediment size that determines channel morphology. In: *Dynamics of Gravel Bed Rivers*. P.Billi, R.D. Hey, C.R. Thorne and P. Tacconi (eds.). John Wiley and Sons, Chichester. pp. 297-311.

Limerinos, J.T. 1970. Determination of the Manning coefficient from measured bed roughness in natural channels. WATER SUPPLY PAPER 1898-B, U.S. Geological Survey, Washington, D.C. 47p.

Manly, B.F. 1991. *Randomization and Monte Carlo Methods in Biology*. Chapman and Hall, New York, NY. 281 pp.

Meyer-Peter, E., and Müller, R. 1948. Formulas for bed-load transport. Proc. 2d Meeting IAHR, Stockholm, pp. 39-64.

Milhous, R.T. 1973. Sediment transport in a gravel-bottomed stream. Ph.D. Thesis. Oregon State University, Corvallis, OR.

Miller, M.C., McCave, I.N. and Komar, P.D. 1977. Threshold of sediment motion in unidirectional currents. SEDIMENTOLOGY, 24: 507-528.

Mosteller, F. and Tukey, J.W. 1977. *Data Analysis and Regression, A Second Course in Statistics*. Addison-Wesley, Reading, MA. 588 pp.

Ott, R.L. 1992. *An Introduction to Statistical Methods and Data Analysis*. Fourth Edition.Wadsworth, Inc., Belmont, CA. 1051 pp.

Parker, G. and Klingeman, P.C. 1982. On why gravel bed streams are paved. WATER RESOURCES RESEARCH, 18:1409-1423.

Parker, G., Klingeman, P.C., and McLean, D.G. 1982. Bedload and size distribution in paved gravel-bed streams. JOURNAL OF THE HYDRAULICS DIVISION, ASCE. Vol. 108. No. HY4. pp. 544-571.

Porth, L.S. 1997. Streamflow estimation: a case study in sample size determination. MS thesis. Colorado State University, Fort Collins, CO. 79 pp.

Rantz, S.E. 1982. Measurement and computation of streamflow: Volume 2. Computation of discharge. U.S. Geological Survey Water Supply Paper 2175. Washington, D.C. 284 pp.

Reid, I., Frostick, L.E., and Layman, J.T. 1985. The incidence and nature of bedload transport during flood flows in coarse-grained alluvial channels. EARTH SURFACE PROCESSES AND LANDFORMS, 10:33-44.

Reid, I. and Frostick, L.E. 1986. Dynamics of bedload transport in Turkey Brook, a coarse-grained alluvial channel. EARTH SURFACE PROCESSES AND LANDFORMS, 11:143-155.

Rubey, W.W. 1933. Setttling velocities of gravel, sand, and silt. AMERICAN JOURNAL OF SCIENCE. Vol. 25. 148:325-338.

Shields, A. 1936. Application of similarity principles and turbulent research to bed-load movement. Berlin: Mitteilungen der Preussische Versuchanstalt fur Wasserbau und Schiffbau, v.26, 26p. [translated by W.P. Ott and J.C. van Uchlen, U.S. Dept. Agriculture, Soil Consv. Service Coop. Lab., Calif. Inst. Tech.].

Simons, D.B. and Sentürk, F. 1992. *Sediment Transport Technology: Water and Sediment Dynamics*. Water Resources Publications, Littleton, CO. 897 pp.

Vanoni, V.A. 1964. Measurements of critical shear stress for entraining fine sediments in a boundary layer. Report KH-R-7. W.M. Keck Lab. of Hydraulics and Water Resources. California Institute of Technology. Pasadena, CA. 47 pp.

Wiberg, P.L. and Smith, J.D. 1987. Calculation of critical shear stress for motion of uniform and hetergeneous sediments. WATER RESOURCES RESEARCH, 23(8): 1471-1480.

Winema National Forest. 1999. Draft U.S. Forest Service Favorable Conditions of Flow in the Upper Klamath Basin. A report prepared by the Water Resources Team, Winema National Forest, Klamath Falls, OR. 48 pp.

Wohl, E.E., Anthony, D.J., Madsen, S.W. and Thompson, D.M. 1996. A comparison of surface sampling methods for coarse fluvial sediments. WATER RESOURCES RESEARCH, 32(10): 3219-3226.

Wolman, M.G. 1954. A method of sampling coarse bed material. AMERICAN GEOPHYSICAL UNION, TRANSACTIONS, 35:951-956.

Yalin, M.S. and Karahan, E. 1979. Inception of sediment transport. JOURNAL OF THE HYDRAULICS DIVISION, ASCE. Vol. 105, No. HY11. pp. 1433-1443.